JEM Journal of Experimental Medicine

ARTICLE

MERTK on mononuclear phagocytes regulates T cell antigen recognition at autoimmune and tumor sites

Robin S. Lindsay[1,2*], Jennifer C. Whitesell[1,2,3*], Kristen E. Dew[2], Erika Rodriguez[2,3], Adam M. Sandor[1,2], Dayna Tracy[2], Seth F. Yannacone[2], Brittany N. Basta[3], Jordan Jacobelli[1,2,3], and Rachel S. Friedman[1,2,3]

Understanding mechanisms of immune regulation is key to developing immunotherapies for autoimmunity and cancer. We examined the role of mononuclear phagocytes during peripheral T cell regulation in type 1 diabetes and melanoma. MERTK expression and activity in mononuclear phagocytes in the pancreatic islets promoted islet T cell regulation, resulting in reduced sensitivity of T cell scanning for cognate antigen in prediabetic islets. MERTK-dependent regulation led to reduced T cell activation and effector function at the disease site in islets and prevented rapid progression of type 1 diabetes. In human islets, MERTK-expressing cells were increased in remaining insulin-containing islets of type 1 diabetic patients, suggesting that MERTK protects islets from autoimmune destruction. MERTK also regulated T cell arrest in melanoma tumors. These data indicate that MERTK signaling in mononuclear phagocytes drives T cell regulation at inflammatory disease sites in peripheral tissues through a mechanism that reduces the sensitivity of scanning for antigen leading to reduced responsiveness to antigen.

Introduction

Mechanisms of immune regulation function at all stages of the immune response to maintain and restore self-tolerance. These checkpoints provide layers of protection to control a normal immune response following pathogen clearance and protect normal tissues from autoimmune destruction. These mechanisms of immune regulation also have the side effect of protecting many tumors from the immune response. The importance of understanding the multiple layers of immune regulation is highlighted by the fact that only 18–36% of cancer patients respond to the targeting of a single checkpoint molecule (Hodi et al., 2010; Topalian et al., 2012), and response rates are improved by targeting multiple checkpoint molecules (Larkin et al., 2015). Thus, altering immune regulation for therapeutic purposes is likely to involve multiple pathways in most cancer and autoimmune patients.

Many layers of immune tolerance must be broken before autoimmune pathology occurs. Type 1 diabetes (T1D) is largely caused by the T cell–mediated autoimmune destruction of the pancreatic islets. We have shown that the T cell response in islets is temporally regulated. Antigenic restimulation of T cells occurs in early stages of islet infiltration, leading to pathogenic T cell effector function, followed by suppression of T cell pathogenesis as islet infiltration advances (Friedman et al., 2014; Lindsay et al., 2015). This T cell regulation in islets eventually fails in mice that present with overt T1D. The mechanisms that drive this temporally controlled regulation of T cell pathogenesis at the disease site in islets are still mostly unknown. This period of T cell regulation is important, because it could represent a novel tolerance checkpoint in islets during T1D progression. Establishing and maintaining tolerance in islets following infiltration is a critical step toward halting disease progression after the autoimmune response has been initiated. Understanding the mechanism by which T cells are regulated in islets during advanced infiltration must be accomplished before we can target this pathway to therapeutically protect tissues from ongoing autoimmune attack.

This period of T cell regulation in advanced infiltrated islets is associated with a loss of antigen-mediated T cell arrest and transient rather than sustained interactions with APCs (Lindsay et al., 2015; Friedman et al., 2014). T cell arrest and sustained interactions with APCs are generally associated with antigen recognition and stimulation, while T cell regulation or tolerance is associated with a lack of T cell arrest and transient APC interactions (Jacobelli et al., 2013; Hugues et al., 2004; Katzman et al., 2010; Shakhar et al., 2005). For example, T cell tolerance through prevention of antigen-mediated T cell arrest has been

[1]Department of Immunology & Microbiology, University of Colorado Anschutz Medical Campus, Aurora, CO; [2]Department of Biomedical Research, National Jewish Health, Denver, CO; [3]Barbara Davis Center for Diabetes, Aurora, CO.

*R.S. Lindsay and J.C. Whitesell contributed equally to this paper; Correspondence to Rachel S. Friedman: rachel.s.friedman@cuanschutz.edu.

shown to be mediated by factors such as regulatory T cells (Tadokoro et al., 2006; Tang et al., 2006) and coinhibitory pathways, including the programmed death 1 (PD-1) pathway (Fife et al., 2009). Notably, we have shown that in the rat insulin promotor (RIP)–membrane-bound OVA (mOva) model of T1D, blockade of PD-1 is not sufficient to restore antigen-mediated T cell arrest in advanced insulitis (Friedman et al., 2014). Thus, the mechanism by which T cells are suppressed in islets during advanced stages of infiltration is unknown.

In order for T cells to form productive interactions with APCs displaying cognate antigen, T cells must navigate and search for antigen in a complex environment with a variety of cues using tightly controlled mechanisms. These cues, which can regulate the sensitivity to antigen, include ligands for adhesion molecules, the physical characteristics of the tissue, chemokines and cytokines, costimulatory and coinhibitory molecules, and presented antigen. The balance of these cues controls the efficiency versus the sensitivity of the T cell response to antigen by altering the number of APCs or targets searched and the thoroughness with which the APCs or targets are scanned (Krummel et al., 2016; Fowell and Kim, 2021).

Mononuclear phagocytes play a key role in the induction of T1D and its pathogenesis, but their role in modulating the immune response in the pancreatic islets during T1D is less clear. Resident and infiltrating mononuclear phagocytes are present in islets during T1D, with the majority of both resident and infiltrating populations expressing CD11c (Jansen et al., 1994; Melli et al., 2009; Calderon et al., 2015; Friedman et al., 2014). Islet-resident mononuclear phagocytes are composed of macrophages and a minor population of CD103$^+$ dendritic cells (DCs; Yin et al., 2012; Friedman et al., 2014), while islet-infiltrating mononuclear phagocytes are monocyte derived (Klementowicz et al., 2017) and contain macrophages and DCs (Zakharov et al., 2020). CD11c-depletion studies indicate that CD11c$^+$ populations have a role in driving disease at early stages of T1D, while at later stages, CD11c$^+$ cells may slow disease progression (Saxena et al., 2007). This dichotomy could be due to temporal changes in CD11c$^+$ populations (Zakharov et al., 2020) and/or differing roles of CD11c$^+$ cells in different tissue locations (i.e., pancreatic LN [PLN] vs. islets). The requirement for BatF3-dependent DCs for the initial break in T cell tolerance in the draining PLNs explains the requirement for CD11c$^+$ cells before insulitis (Ferris et al., 2014; Gagnerault et al., 2002; Turley et al., 2003). CD11c$^+$ cells also dramatically enhance entry of lymphocytes into inflamed islets, providing another potential node of disease regulation (Sandor et al., 2019). Yet, following the initial break in immunological tolerance the role of mononuclear phagocytes within islets has not been elucidated. The fact that T1D progression is not altered by the removal of the draining PLNs following the establishment of insulitis (Gagnerault et al., 2002) suggests that the disease site in islets may be the relevant site to interrogate. The function of the mononuclear phagocytes in islets at different stages of islet infiltration is not clear.

MERTK, which is best known as a macrophage marker, is expressed on mononuclear phagocytes, where its signaling plays an immunoregulatory role. MERTK is a member of the TAM (TYRO3 AXL MERTK) family of receptor tyrosine kinases. TAM receptors and their ligands function in phagocytosis of apoptotic cells, tolerance induction, coagulation, and erythropoiesis (Lu and Lemke, 2001; Nagata et al., 1996; Nakano et al., 1997; Scott et al., 2001; van der Meer et al., 2014; Rothlin et al., 2015). MERTK-mediated apoptotic cell uptake results in immunoregulation of APCs and production of inflammation resolution mediators (Wallet et al., 2008; Cai et al., 2018). MERTK has also been implicated in T cell tolerance induction to self-antigens expressed by apoptotic β cells in the nonobese diabetic (NOD) model (Wallet et al., 2008). It has been suggested that MERTK might be a checkpoint molecule that could be targeted to intervene in immune tolerance (Akalu et al., 2017; Cook et al., 2013), yet its role as such has not yet been clearly defined.

Having previously identified a transient regulation of T cells in T1D, we sought to identify the mediator of this immune regulation through interrogating the mechanism by which T cells are suppressed at the autoimmune disease site. Using in vivo imaging of pancreatic islets, we found that CD11c$^+$ cells prevent T cells from arresting and responding to their antigen via a MERTK-dependent mechanism. This result was mirrored in a solid tumor model, indicating the broad applicability of this mechanism. MERTK inhibition or deficiency drove decreased T cell motility leading to enhanced T cell scanning for cognate antigen and increased antigen-dependent sustained interactions of T cells with CD11c$^+$ APCs. This led to a very rapid increase in antigen experience and lytic potential by islet-infiltrating T cells, which was restricted to the disease site. The increased T cell activation in islets resulted in the rapid onset of T1D in animals with preexisting insulitis. Increased numbers of MERTK-expressing cells were also observed in the remaining intact islets of T1D patients. These data indicate that MERTK signaling in mononuclear phagocytes is driving tissue protective T cell regulation specifically at autoimmune and tumor disease sites.

Results

CD11c$^+$ cells mediate the suppression of T cell arrest in islets

We previously identified temporally controlled periods of T cell stimulation and suppression in islets (Friedman et al., 2014; Lindsay et al., 2015). Advanced stages of islet infiltration were dominated by T cell regulation, which was characterized by a loss of antigen-mediated T cell arrest, pathogenic cytokine production, and interactions with CD11c$^+$ cells (Friedman et al., 2014; Lindsay et al., 2015). Since DCs, macrophages, and monocytes all have the potential to drive T cell tolerance, we hypothesized that a subset of CD11c$^+$ cells is responsible for this T cell regulation in advanced infiltrated islets. To test this hypothesis, we generated mixed bone marrow (BM) chimeras using NOD.CD11c-DTR (diphtheria toxin [DT] receptor) BM with either fluorescent islet-antigen–specific 8.3 CD8 T cells (Fig. 1, A–G; and Video 1) or fluorescent polyclonal NOD T cells (Fig. 1, H–K). 5–10% fluorescently labeled T cells were used to enable tracking of individual T cells. The chimeric mice were treated with two doses of DT to deplete the CD11c$^+$ cells or vehicle (PBS) as a control (Sandor et al., 2019). 48 h after the initial treatment, islets were isolated for analysis (Fig. 1, A and H). We confirmed that CD11c depletion was effective in islets (Fig. S1 A). The

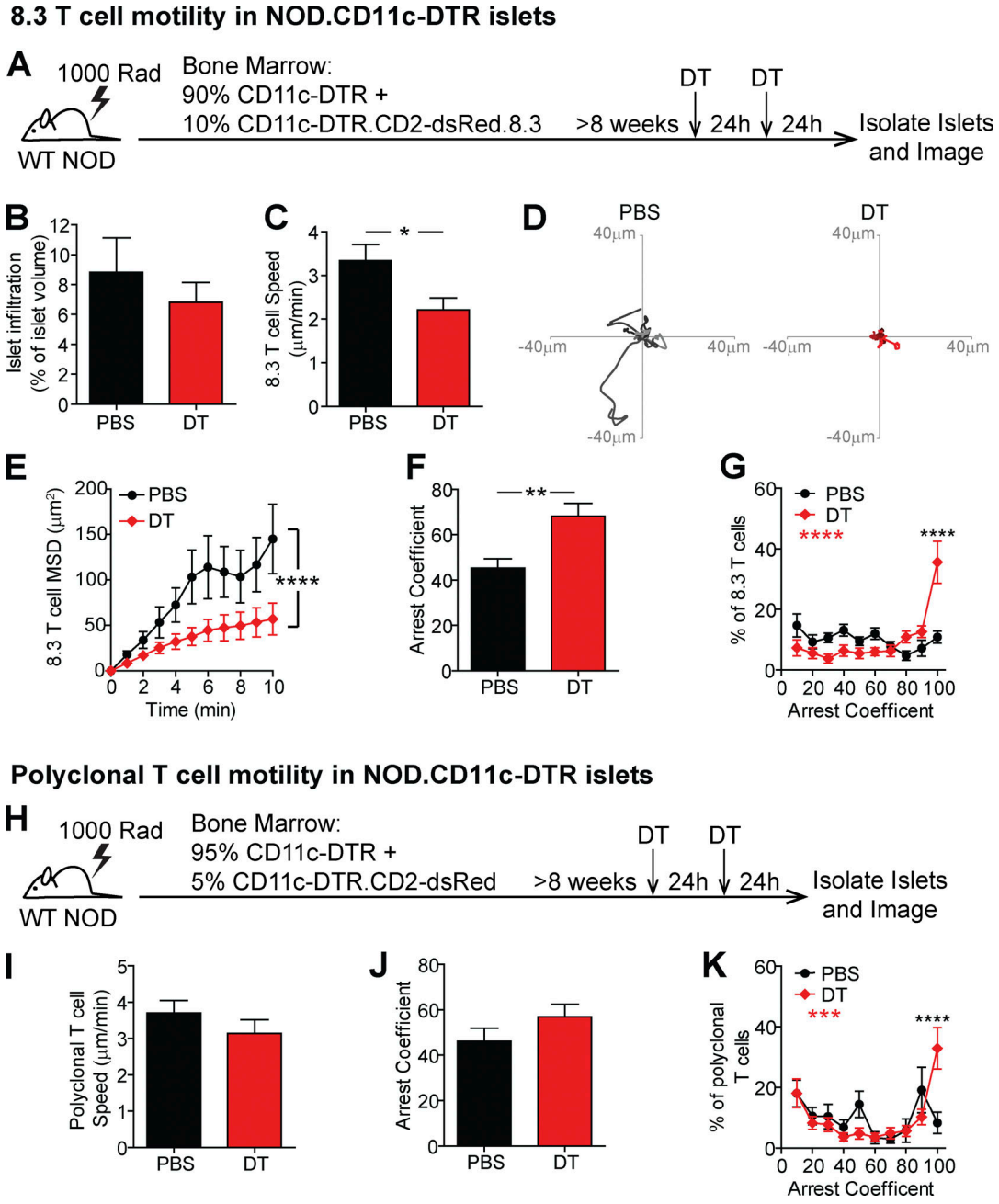

Figure 1. **CD11c⁺ cells in islets prevent T cell arrest. (A–K)** NOD.CD11c-DTR BM chimeras containing 90% NOD.CD11c-DTR BM + 10% NOD.CD11c-DTR.8.3.CD2-dsRed BM (A–G) or 95% CD11c-DTR + 5% CD11c-DTR.CD2-dsRed (H–K) were treated twice with PBS (control) or DT (CD11c depleted). **(A and H)** Schematic of experimental setup to analyze T cell motility in explanted islets by two-photon microscopy. **(B)** Average level of islet infiltration. **(C and I)** Average T cell crawling speed per islet. **(D)** Example of representative 15-min tracks of motion of 15 randomly selected T cells from individual islets. **(E)** MSD over time indicates the T cells' ability to translocate away from their place of origin, averaged per islet. **(F, G, J, and K)** Arrest coefficient, or the percentage of time a T cell is moving <1.5 µm/min, averaged per islet. **(A–K)** Data are pooled from three independent experiments, and error bars represent SEM. **(A–G)** *n* = 10 islets containing 647 analyzed 8.3 T cells from PBS treated mice and *n* = 11 islets containing 371 analyzed 8.3 T cells from DT treated mice. **(H–K)** *n* = 13 islets containing 156 analyzed polyclonal T cells from PBS treated mice and *n* = 15 islets containing 329 analyzed polyclonal T cells from DT treated mice. **(B, C, F, I, and J)** Statistics: Student's t test. **(E, G, and K)** Statistics: two-way ANOVA with Bonferroni's multiple comparison test, treatment effect (black statistic), interaction effect (red statistic). **(B–K)** *, P < 0.05; **, P < 0.01; ***, P < 0.001; ****, P < 0.0001.

population depleted included most of the islet mononuclear phagocyte compartment, including CD11b⁺, XCR1⁺, and MERTK⁺ populations (Fig. S1 B).

The ex vivo method of explanted islet imaging recapitulates T cell behavior in islets within the intact pancreas of live animals (Lindsay et al., 2015). The infiltration state of each islet analyzed was quantified to ensure that equivalent islets were analyzed in the intact and CD11c-depleted conditions (Fig. 1 B), since T cell behavior varies with the level of T cell infiltration (Lindsay et al., 2015; Friedman et al., 2014).

The depletion of CD11c$^+$ cells resulted in significantly decreased islet-antigen–specific 8.3 CD8 T cell crawling speed within islets (Fig. 1, C and D; and Video 1). The reduced crawling speed resulted in significantly reduced T cell translocation from the point of origin, as indicated by the mean squared displacement (MSD) over time (Fig. 1 E). Furthermore, the 8.3 T cells in islets showed greater arrest as indicated by an increased arrest coefficient (percentage of time a T cell spends crawling <1.5 µm/min; Fig. 1, F and G). There was a highly significant increase in the frequency of fully arrested T cells (arrest coefficient of 100; Fig. 1 G). Notably, we previously determined that T cell arrest in islets is antigen dependent and correlated with increases in both T cell–APC interactions and T cell effector functions in islets (Lindsay et al., 2015; Friedman et al., 2014), suggesting that the depletion of islet CD11c$^+$ cells may be promoting T cell restimulation.

To determine whether CD11c$^+$ cells have a similar effect on the motility and arrest of endogenous polyclonal CD4 and CD8 T cells in islets, we depleted CD11c$^+$ cells in mice with fluorescently labeled polyclonal T cells (Fig. 1 H). The average T cell crawling speed (Fig. 1 I) and average T cell arrest coefficient (Fig. 1 J) were not significantly different between CD11c-depleted and intact mice. This suggests that the CD11c$^+$ cell–dependent change in islet T cell motility is dependent on islet-antigen specificity. However, there was a highly significant increase in fully arrested T cells (arrest coefficient of 100) following CD11c$^+$ cell depletion (Fig. 1 K), suggesting that a subset of islet-antigen–specific polyclonal T cells is responding to CD11c$^+$ cell depletion.

These data suggest that in the absence of suppressive CD11c$^+$ cells, CD8 T cells are able to respond to antigen presented by other cells in islets, such as β cells, CD11c$^-$ macrophages, or B cells, resulting in T cell arrest. The reduced effect on polyclonal T cells at a population level is likely due to the presence of nonislet-antigen–specific T cells in islets and also the inability of CD4 T cells to recognize antigen on MHC class II$^-$ β cells. These data indicate that CD11c$^+$ cells play a dominant role in preventing T cell arrest on APCs or β cells in islets.

DCs can have the potential to be either stimulating or tolerogenic. We next sought to determine whether Zbtb46-expressing classical DCs within islets were responsible for regulating T cell arrest. Due to the availability of Zbtb46-DTR mice on the C57BL/6 background, we chose to use the RIP-mOva system in which a mOva is expressed in the β cells under the RIP. We generated BM chimeras using B6.Zbtb46-DTR (Meredith et al., 2012) BM transferred into irradiated C57BL/6.RIP-mOva recipients (Fig. S2 A). In this system the transfer of OVA-specific OT-I CD8 T cells induces T cell infiltration of islets (Kurts et al., 1997). Our previous work has shown that islet-antigen–specific OT-I T cells in RIP-mOva islets show the same dynamics of response as islet-antigen–specific CD4 and CD8 T cells in the islets of NOD mice, including a period of T cell suppression in advanced infiltrated islets (Friedman et al., 2014). T cell infiltration of islets was induced in RIP-mOva.Zbtb46-DTR chimeric mice by transfer of naive OT-I.Ubiquitin-GFP T cells. 3–5 d following OT-I T cell transfer, the chimeric mice were treated with two doses of DT to deplete classical DCs or two doses of vehicle (PBS) as a control. 48 h after the initial dose, islets were isolated and imaged by two-photon microscopy (Fig. S2 A). No differences were seen in the islet-antigen–specific T cell crawling speed (Fig. S2 B) or arrest (Fig. S2 C) following classical DC depletion, despite equivalent infiltration of the islets analyzed (Fig. S2 D). Analysis of islet mononuclear phagocyte populations following depletion in Zbtb46-DTR chimeras showed that XCR1$^+$ cDC1s were significantly reduced, while CD11b$^+$ and MERTK$^+$ populations remained intact (Fig. S2 E). These data indicate that classical DCs are not required for the T cell regulation mediated by CD11c$^+$ cells in islets.

MERTK is expressed on islet CD11c$^+$ cells

Since CD11c$^+$ cell–mediated T cell regulation was not dependent on classical DCs, we sought to understand the source of the regulation in macrophage and monocyte populations. Monocyte-derived CD11c$^+$ cells infiltrate islets together with T cells (Melli et al., 2009; Jansen et al., 1994; Klementowicz et al., 2017). MERTK is expressed on macrophages and some monocytes in peripheral tissues (Guilliams et al., 2014; Tamoutounour et al., 2013), mediates immunoregulation of APCs, and has been implicated in T cell tolerance (Cabezón et al., 2015; Cook et al., 2013), including in the NOD model (Wallet et al., 2008).

We previously identified CX3CR1 levels as a marker to distinguish resident CD11c$^+$ cells from infiltrating CD11c$^+$ cells (Friedman et al., 2014). Here, we show that in NOD islets, the numbers of islet-infiltrating CX3CR1^{low} CD11c$^+$ cells directly correlated with total levels of islet infiltration (Fig. 2, A–C). MERTK was expressed on both islet-resident (CX3CR1^{high}) and islet-infiltrating (CX3CR1^{low}) CD11c$^+$ cells in the NOD model (Fig. 2, A, B, and D), and as previously observed, MERTK-expressing CD11c$^+$ cells increased with increasing islet infiltration (Fig. 2 E; Mohan et al., 2017). Thus, based on the increased frequency of MERTK-expressing CD11c$^+$ cells in advanced infiltrated islets, we sought to determine if MERTK signaling was responsible for driving T cell regulation.

MERTK regulates islet T cell motility and arrest in a T cell–extrinsic manner

To test the hypothesis that MERTK signaling in mononuclear phagocytes promotes T cell regulation in infiltrated islets, we analyzed WT T cell motility in islets of WT NOD versus NOD.MERTK$^{-/-}$ mice. CD11c$^+$ and CD11b$^+$ mononuclear phagocyte frequency in islets was not altered by MERTK deficiency (Fig. S3 A). However, NOD.MERTK$^{-/-}$ mice have altered thymic selection, which results in the absence of T1D and strongly diminished spontaneous insulitis (Wallet et al., 2009). Thus, to induce islet infiltration, we transferred in vitro–activated BDC-2.5 T cells into WT NOD and NOD.MERTK$^{-/-}$ recipients. 3–6 d later, fluorescently labeled activated 8.3 CD8 T cells and BDC-2.5 CD4 T cells were transferred into the same hosts. 24 h after fluorescent T cell transfer, islets were isolated and analyzed by two-photon microscopy (Fig. 3, A and B; and Video 2). WT and MERTK$^{-/-}$ islets analyzed had equivalent infiltration (Fig. 3 C). Islet-antigen–specific CD8 and CD4 T cell motility was significantly reduced in islets of MERTK$^{-/-}$ recipients compared with WT recipients (Fig. 3, D, E, I, and J; and Video 2). The motility of

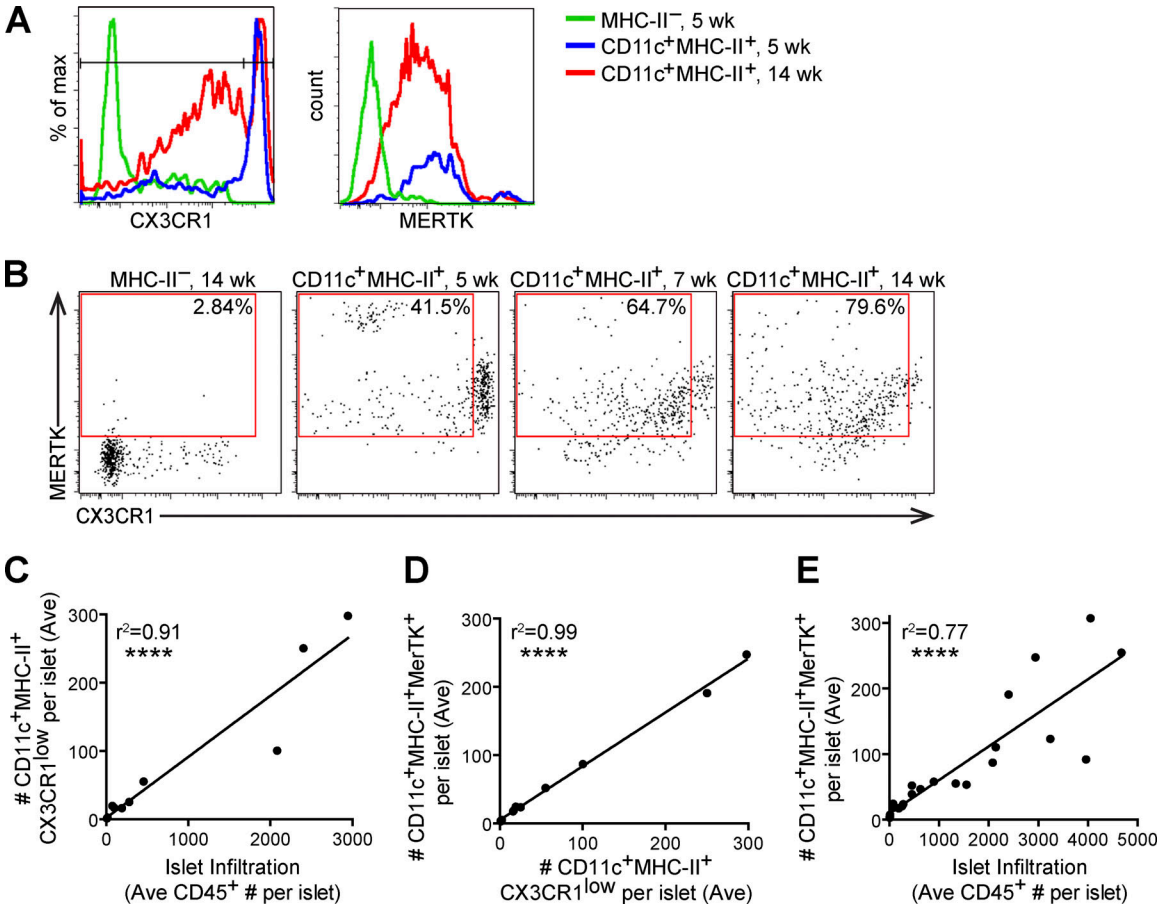

Figure 2. **MERTK-expressing cells increase with progression of islet infiltration.** Islets from 4–18-wk-old NOD or NOD.CX3CR1-GFP female mice were isolated, digested and dissociated, stained, and analyzed by flow cytometry. **(A)** Example histograms of CX3CR1 gating in female NOD.CX3CR1-GFP islets. **(B)** Example plots of MERTK$^+$CX3CR1^{Low} gating in female NOD islets, with percentage of positive in the gate shown. **(C–E)** Each dot represents one mouse, as the number of cells in the islets normalized to the number of islets per mouse (Ave). **(C)** Quantification of CD11c$^+$MHC-II$^+$CX3CR^{low} (infiltrating APCs) versus the leukocyte infiltration in islets. **(D)** Quantification of CD11c$^+$MHC-II$^+$MERTK$^+$ cells versus CX3CR1^{low} CD11c$^+$MHC-II$^+$ infiltrating APCs in islets. **(E)** MERTK$^+$CD11c$^+$MHC-II$^+$ versus leukocyte infiltration in islets. *n* = 11 mice from two independent experiments (A–D); *n* = 24 mice from six independent experiments (E). Statistics calculated by Pearson correlation; ****, P < 0.0001 (C–E).

the CD8 and CD4 T cells was also more confined in MERTK$^{-/-}$ islets, as determined by the MSD (Fig. 3, F and K). This was accompanied by a significant increase in T cell arrest in MERTK$^{-/-}$ islets (Fig. 3, G and L) with an increased frequency of fully arrested T cells in islets of MERTK$^{-/-}$ mice (Fig. 3, H and M). The increased T cell arrest observed in MERTK$^{-/-}$ hosts suggests that MERTK signaling in MERTK-expressing CD11c$^+$ cells drives the T cell–extrinsic regulation of T cell arrest in infiltrated islets.

MERTK signaling promotes T cell motility in infiltrated islets independent of cognate antigen

To determine whether MERTK signaling promotes T cell regulation in an antigen-dependent or independent manner, we treated mice orally with UNC2025, a highly selective inhibitor of MERTK and Flt3 (Zhang et al., 2014). To ensure that UNC2025 was not reducing the CD11c$^+$ or MERTK$^+$ population in islets via Flt3 inhibition, MERTK inhibition, or off-target effects, we analyzed the frequency of CD11c$^+$ APCs and MERTK-expressing CD11c$^+$ APCs in islets following 4 wk of continuous twice-daily oral treatment with 30 mg/kg UNC2025. There was no significant difference in these populations following 4 wk of treatment (Fig. S3 B); thus, we extrapolate that UNC2025 is not altering the frequency of the CD11c populations in islets following short-term treatment.

To analyze islet-antigen–specific T cell and polyclonal T cell motility, arrest, and displacement in islets, we cotransferred activated, fluorescently labeled, islet-antigen–specific 8.3 CD8 T cells, islet-antigen–specific BDC-2.5 CD4 T cells, and polyclonal NOD T cells into NOD.CD11c-YFP hosts. These recipient mice were treated with UNC2025 or vehicle for 16 h, and isolated islets were imaged by two-photon microscopy (Fig. 4 A). The UNC2025 and vehicle-treated islets analyzed were matched for level of infiltration (Fig. 4 B). Following UNC2025 treatment, there was a significant decrease in islet-antigen–specific CD8 and CD4 T cell crawling speed as well as polyclonal NOD T cell crawling speed (Fig. 4 C). This was accompanied by increased T cell arrest in islet-antigen–specific and polyclonal T cells (Fig. 4, D and E). Islet-antigen–specific CD8 and CD4 T cells showed a highly significant increase in fully arrested T cells following

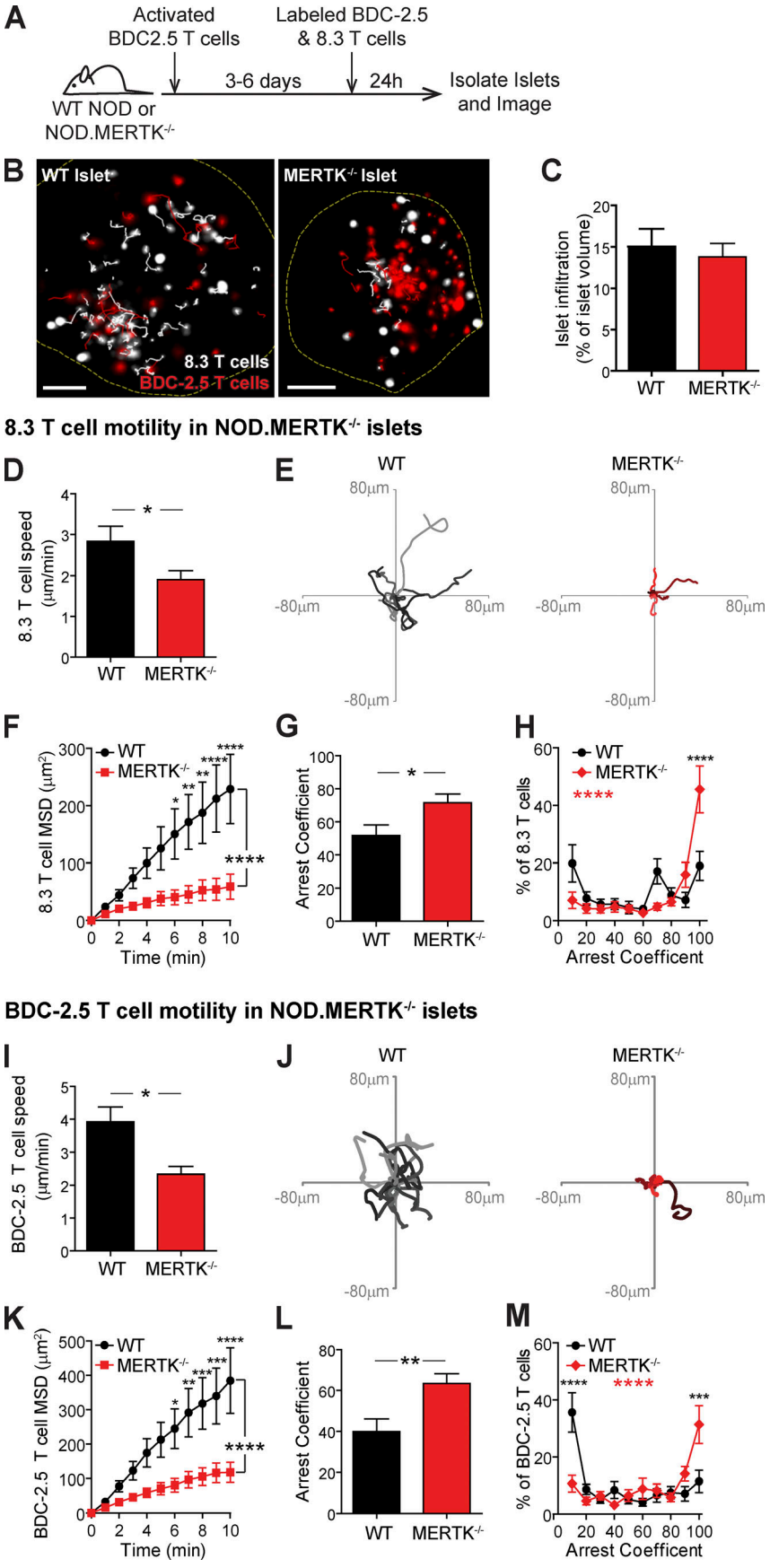

Figure 3. **Islet-antigen–specific T cells in MERTK$^{-/-}$ islets show decreased motility and increased T cell arrest.** Activated BDC-2.5 CD4 T cells were transferred into NOD or NOD.MERTK$^{-/-}$ female mice to initiate islet infiltration. Fluorescently labeled activated 8.3 CD8 and BDC-2.5 CD4 T cells were then transferred into the same mice 3–6 d later. 24 h after fluorescent T cell transfer, islets were isolated and analyzed by two-photon microscopy. **(A)** Schematic of experimental setup. **(B)** Representative islet images from WT NOD or NOD.MERTK$^{-/-}$ mice with 10-min tracks of motion. Dashed line depicts islet border. 8.3 CD8 T cells are shown in white, and BDC-2.5 CD4 T cells are shown in red. Scale bars, 50 µm. **(C)** Average level of islet infiltration. **(D and I)** Average T cell crawling speed per islet. **(E and J)** Example of representative 15-min tracks of motion of 15 T cells from representative islets. **(F and K)** MSD over time, averaged per islet. **(G, H, L, and M)** Arrest coefficient: percentage of time that a cell crawls <1.5 µm/min, averaged per islet. **(C–M)** Data are pooled from four or five independent experiments. Error bars represent SEM. **(D–H)** n = 22 WT islets containing 864 analyzed 8.3 T cells and n = 23 MERTK$^{-/-}$ islets containing 893 analyzed 8.3 T cells. **(I–M)** n = 25 WT islets containing 1,069 analyzed BDC-2.5 T cells and n = 28 MERTK$^{-/-}$ islets containing 1496 analyzed BDC-2.5 T cells. **(C, D, G, I, and L)** Statistics: two-tailed Student's t test. **(F, H, K, and M)** Statistics: two-way ANOVA with Bonferroni's multiple comparison test, treatment effect (black statistic), interaction effect (red statistic). *, P < 0.05; **, P < 0.01; ***, P < 0.001; ****, P < 0.0001.

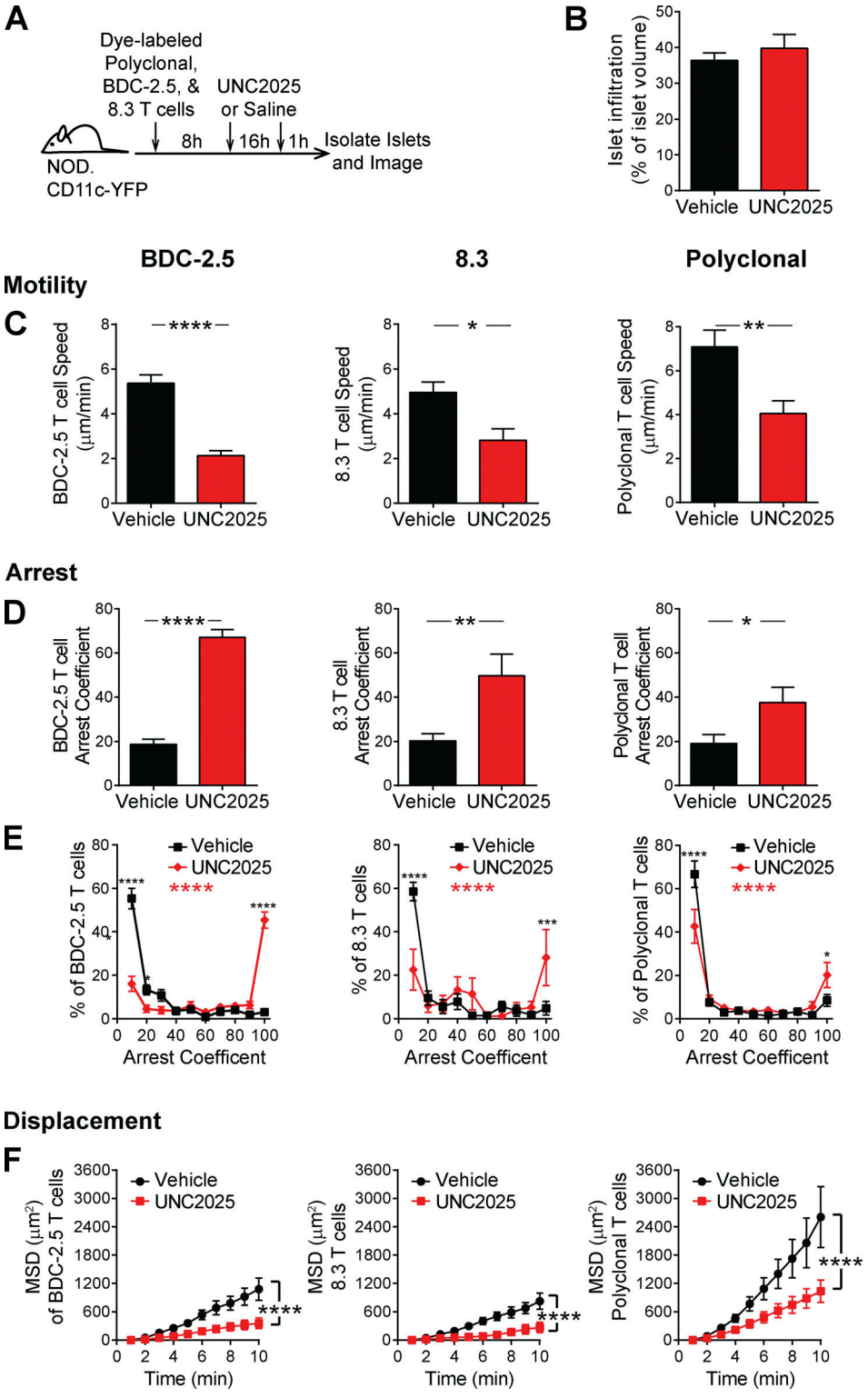

Figure 4. **MERTK signaling drives antigen-independent suppression of T cell arrest in islets.** Activated 8.3 CD8 T cells, BDC-2.5 CD4 T cells, and polyclonal T cells were fluorescently labeled and cotransferred into female NOD.CD11c-YFP mice. Mice were treated twice daily with saline vehicle or 30 mg/kg UNC2025, a small-molecule inhibitor of MERTK and Flt3. 17 h following the initial treatment, islets were isolated and analyzed by two-photon microscopy. **(A)** Schematic of experimental setup. **(B)** Average level of islet infiltration. **(C)** Average T cell crawling speed per islet. **(D and E)** Arrest coefficient: percentage of time that a cell crawls <1.5 µm/min, averaged per islet. **(F)** MSD over time indicates the T cells' ability to translocate away from their place of origin, averaged per islet. **(A–F)** n = 17 islets from vehicle-treated mice containing 590 analyzed BDC-2.5 T cells, 182 analyzed 8.3 T cells, and 497 analyzed polyclonal T cells. n = 8–11 islets from UNC2025 treated mice containing 481 analyzed BDC-2.5 T cells, 49 analyzed 8.3 T cells, and 671 analyzed polyclonal T cells. Data were derived from two or three independent experiments. **(B–D)** Statistics: two-tailed Student's t test. Error bars represent SEM. **(E and F)** Statistics: two-way ANOVA with Bonferroni's multiple comparison test, treatment effect (black statistic), interaction effect (red statistic); *, P < 0.05; **, P < 0.01; ***, P < 0.001; ****, P < 0.0001. Error bars represent SEM.

UNC2025 treatment, while polyclonal T cells showed a modest increase in the frequency of fully arrested T cells following MERTK inhibition (Fig. 4 E). The movement of islet-antigen–specific and polyclonal T cells was more confined following UNC2025 treatment compared with control saline treatment, as determined by the MSD over time (Fig. 4 F). Notably, mouse T cells do not express MERTK; thus, MERTK-dependent T cell changes are extrinsically mediated by MERTK-expressing CD11c$^+$ cells in islets, as supported by our findings in MERTK$^{-/-}$ mice (Fig. 3). These data indicate that MERTK inhibition by UNC2025 treatment alters T cell motility in an antigen-independent manner. These findings led to the question of whether this MERTK-mediated mechanism of T cell regulation was relevant to diverse disease settings.

MERTK regulates T cell arrest in a solid tumor

Our findings indicate that MERTK signaling in mononuclear phagocytes regulates the T cell response in autoimmunity. Many mechanisms of immune regulation are shared between autoimmune and tumor settings, which led us to ask if regulation by MERTK signaling was altering the tumor-specific T cell response. TAM receptor family member–mediated regulation of the T cell response within the tumor is an active area of clinical and preclinical research (Myers et al., 2019; Wu et al., 2018a; Zhou et al., 2020; Maimon et al., 2021). MERTK-specific inhibition has been shown to suppress tumor growth in murine solid tumor models (Sinik et al., 2019; Wu et al., 2018b; Cook et al., 2013; Zhou et al., 2020). In some solid tumors, MERTK acts through modulation of the local type I IFN response (Zhou et al., 2020). Additionally, suppression of TAM receptor signaling has been shown to increase the response to anti–PD-1 therapy in murine tumor models, suggesting that it is mediated by a mechanism other than PD-1 signaling (Kasikara et al., 2019; Zhou et al., 2020). As a result, we sought to determine if enhanced T cell arrest was also observed in a solid tumor with MERTK deficiency or following MERTK inhibition.

To determine whether MERTK regulates T cell motility in a solid-tumor setting, we analyzed T cell motility and arrest in B78ChOva tumors. We chose the B78ChOva tumor model because it has a high frequency of MERTK-expressing tumor-associated macrophages and expresses OVA (Broz et al., 2014). B78ChOva tumor cells were implanted subcutaneously in C57Bl/6 mice and allowed to grow for 4–6 d. Activated tumor-specific OT-I T cells were then transferred. Following T cell trafficking to the tumor site, mice were treated with either saline or UNC2025 for 18 h. Tumors were then excised and imaged by two-photon microscopy (Fig. 5 A). To ensure that the effect was MERTK specific and show that the effect was specific to the host cells recruited to the tumor, these experiments were repeated comparing WT and MERTK$^{-/-}$ hosts.

The tumor-specific OT-I T cells showed a dramatic change in motility following MERTK inhibition (Fig. 5, B–G) or in MERTK$^{-/-}$ hosts (Fig. 5, H–L). As in advanced infiltrated islets, OT-I T cells on the surface of the tumor were highly motile despite an abundance of local cognate antigen. However, when MERTK signaling was inhibited or deficient, the T cells increased arrest (Fig. 5 and Video 3). Both the T cells and tumor cells that were transferred into MERTK$^{-/-}$ hosts were WT in origin and thus contained an intact MERTK gene. This indicated that host-derived cells, likely MERTK-expressing tumor-associated macrophages, were responsible for the changes in T cell behavior. We next asked whether the T cell arrest promoted by MERTK inhibition was in part associated with increased antigenic stimulation.

MERTK signaling regulates antigen-dependent T cell–APC interactions in islets

While MERTK inhibition or deficiency modulated T cell motility and arrest in islets in an antigen-independent manner, the higher speed and displacement of polyclonal T cells compared with islet-antigen–specific T cells (Fig. 4) raised the question of whether cognate antigen also played a role in this regulation. Previous work has suggested that MERTK-dependent tolerance is mediated by modulation of costimulation, including CD40, CD80, and CD86 (Wallet et al., 2008). We found that these costimulatory ligands and PD-L1 were not modulated on CD11c$^+$ cells in islets by inhibition of MERTK (Fig. S4), suggesting an alternative mechanism of T cell regulation. Thus, we next explored if prevention of interactions between T cells and APCs might be a possible mechanism of MERTK-mediated regulation.

To determine whether antigen-dependent T cell–APC interactions in islets were increased as a result of MERTK inhibition, we analyzed 8.3 CD8 T cell, BDC-2.5 CD4 T cell, and polyclonal T cell interactions with CD11c$^+$ cells following 16 h of UNC2025 treatment (Fig. 6 A). In the LNs, brief T cell–APC interactions have been shown to be tolerogenic, whereas sustained T cell–APC interactions have been shown to be activating (Jacobelli et al., 2013). Thus, we analyzed the duration of T cell–CD11c$^+$ cell interactions and the frequency of sustained interactions longer than 10 min in duration. The frequency of islet-antigen–specific CD4 and CD8 T cells participating in sustained interactions with CD11c$^+$ cells was significantly increased in BDC-2.5 CD4 T cells, while polyclonal T cells showed no change (Fig. 6, C and D; and Video 4). Islet-antigen–specific BDC-2.5 CD4 T cells also showed a significant increase in the duration of interaction with CD11c$^+$ APCs in islets following UNC2025 treatment, while polyclonal T cells showed no change (Fig. 6 E and Video 4). These data suggest that while MERTK signaling alters T cell motility in an antigen-independent manner, it controls T cell interactions with APCs in an antigen-dependent manner by diminishing the efficiency of T cell scanning for cognate antigen.

T cell antigen recognition and effector function are increased following MERTK inhibition

To determine how MERTK-mediated regulation of T cell–APC interactions affected antigen recognition by and activation of T cells in islets and LNs, we analyzed expression of CD44 and CD62L by flow cytometry following 17 h of UNC2025 treatment of NOD mice. Polyclonal CD8 and CD4 T cells in islets showed a rapid and significant increase in antigen experience (CD44^{high}CD62L$^-$) following MERTK inhibition (Figs. 7 A and S5, suggesting that the increased arrest and T cell–APC interactions seen with MERTK inhibition are driving increased antigen

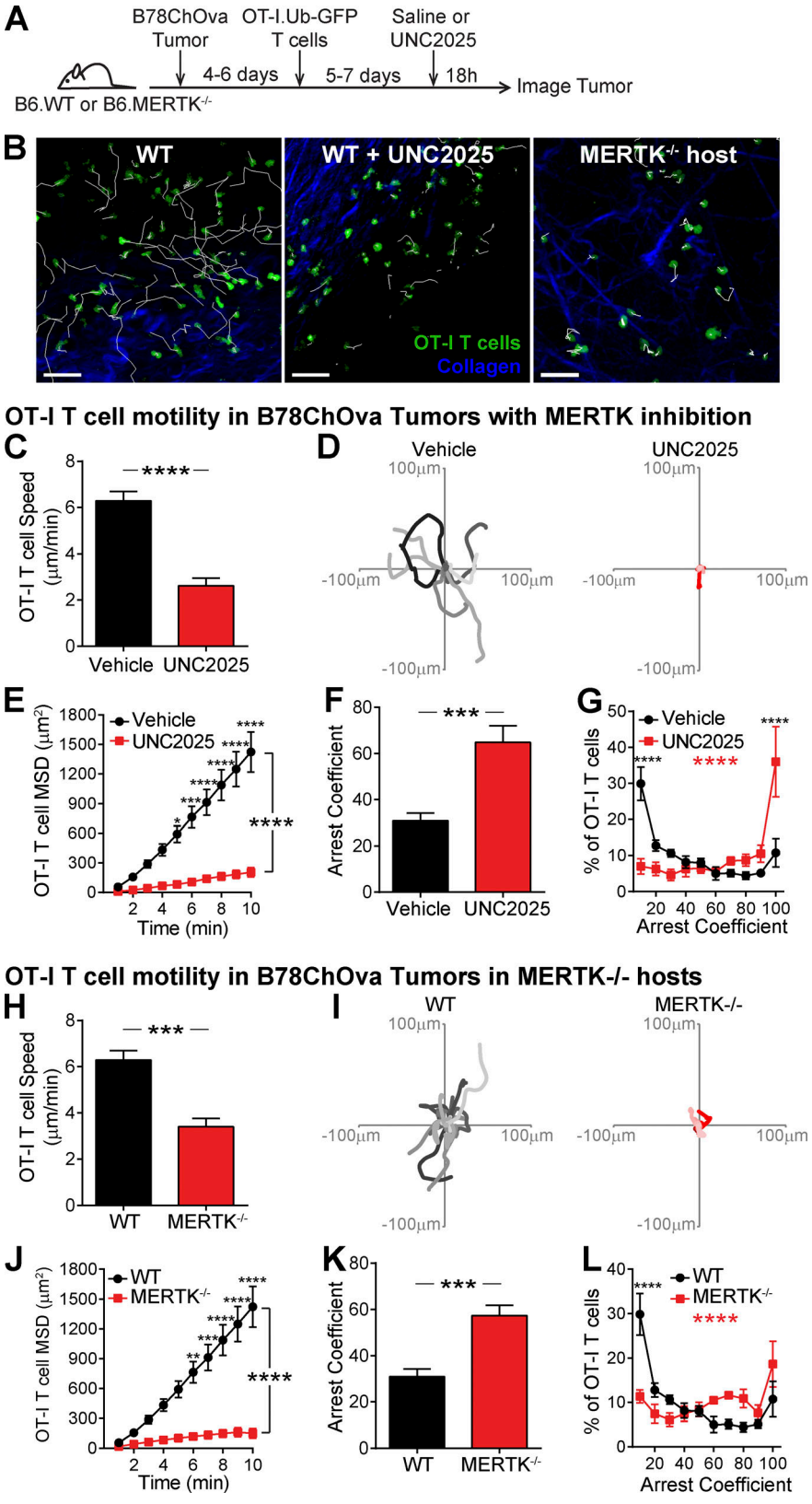

Figure 5. **MERTK signaling in tumor associated host cells prevents tumor-specific T cell arrest in a solid tumor.** B78ChOva tumor cells were implanted in C57BL/6 or C57BL/6.MERTK$^{-/-}$ mice. Activated OT-I.Ubiquitin-GFP CD8 T cells were then transferred into tumor-bearing mice 4–6 d later. 5–7 d after fluorescent T cell transfer, mice were treated with UNC2025 or vehicle. 18 h after treatment, tumors were excised and analyzed by two-photon microscopy. **(A)** Schematic of experimental setup. **(B)** Representative images of OT-I T cell (green) motility on the tumor surface with 10-min tracks of motion. Collagen (blue) delineates the tumor capsule. Scale bars, 50 μm. **(C and H)** Average T cell crawling speed in the tumor, averaged per tumor. **(D and I)** Example representative 15-min tracks of motion of OT-I T cells in representative tumors. **(E and J)** MSD over time, averaged per tumor. **(F, G, K, and L)** Arrest coefficient: percentage of time that a cell crawls <2 μm/min, averaged per tumor. **(B–L)** Data are pooled from three to six independent experiments. Error bars represent SEM. *n* = 10 tumors from WT hosts containing 2,230 analyzed OT-I T cells. *n* = 6 tumors from UNC2025-treated mice containing 1,130 analyzed OT-I T cells. *n* = 5 tumors from MERTK$^{-/-}$ hosts containing 641 analyzed OT-I T cells. **(C, F, H, and K)** Statistics: two-tailed Student's *t* test. **(E, G, J, and L)** Statistics: two-way ANOVA with Bonferroni's multiple comparison test, treatment effect (black statistic), interaction effect (red statistic), *, P < 0.05; **, P < 0.01; ***, P < 0.001; ****, P < 0.0001.

recognition and TCR signaling in islets. Notably, there was no significant difference in antigen experience in draining PLNs or nondraining inguinal LNs (ILNs; Figs. 7 A and S5). These data suggest that MERTK signaling is functioning to suppress the T cell response by preventing antigen recognition specifically at the disease site in islets.

To determine whether effector function was also increased by MERTK inhibition, we analyzed expression of granzyme B in

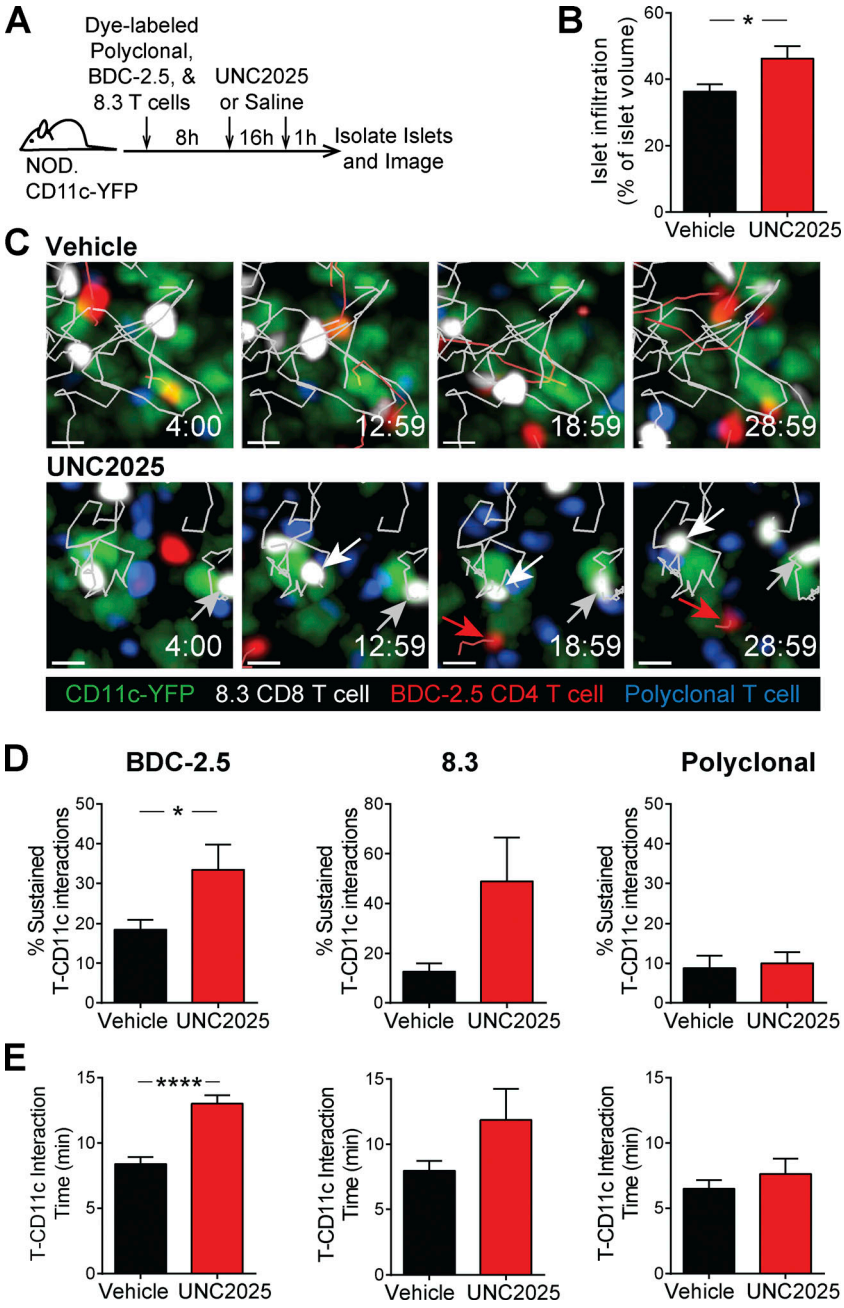

Figure 6. **MERTK signaling drives suppression of antigen-dependent T cell–APC interactions in islets.** Activated 8.3 CD8 T cells (white), BDC-2.5 CD4 T cells (red), and polyclonal T cells (blue) were fluorescently labeled and cotransferred into female NOD.CD11c-YFP mice (green). Mice were treated twice daily with saline vehicle or 30 mg/kg UNC2025. 17 h following the initial treatment, islets were isolated and analyzed by two-photon microscopy. **(A)** Schematic of experimental setup. **(B)** Average level of islet infiltration. **(C)** Representative islet images from vehicle- or UNC2025-treated mice with 5-min tracks of motion. White and gray arrows point to sustained interactions between 8.3 T cells and CD11c cells. Red arrows point to sustained interactions between BDC-2.5 T cells and CD11c cells. **(D)** Percentage of T cells participating in sustained interactions (≥10 min) with CD11c$^+$ cells. Scale bars, 10 µm. **(E)** Average duration of interaction between T cells and CD11c$^+$ cells. **(A–E)** *n* = 16–17 islets from vehicle-treated mice containing 575 analyzed BDC-2.5 T cells, 168 analyzed 8.3 T cells, and 470 analyzed polyclonal T cells. *n* = 8–9 islets from UNC2025 treated mice containing 356 analyzed BDC-2.5 T cells, 60 analyzed 8.3 T cells, and 907 analyzed polyclonal T cells. Data were derived from two or three independent experiments. **(B, D, and E)** Statistics: two-tailed Student's t test; *, P < 0.05; ****, P < 0.0001. Error bars represent SEM.

CD8 T cells by flow cytometry following 17–24 h of UNC2025 treatment of NOD mice. Granzyme B expression serves as an indicator of CD8 T cell activation and lytic potential. Polyclonal CD8 T cells in islets showed a rapid and significant increase in the amount of granzyme B following MERTK inhibition (Fig. 7 B). On the other hand, IFN-γ production was not modulated with MERTK inhibition (data not shown). As seen with antigen experience, there was no significant difference in granzyme B expression in draining PLNs or nondraining ILNs (Fig. 7 B), further indicating that MERTK signaling is acting specifically at the disease site. Notably, only half of the mice showed an increase in CD8 T cell granzyme B, indicating that while T cells in the islets of all mice show increases in antigen experience, other mechanisms of tolerance may control effector function.

Inhibition of MERTK signaling drives rapid T1D induction in mice with existing islet infiltration

To determine how inhibition of MERTK affects T1D progression, we treated NOD mice with UNC2025 or saline vehicle for 17 h and analyzed changes in islet infiltration by quantification of histological staining. The data show a rapid increase in the frequency and degree of islet infiltration after only 17 h of MERTK inhibition (Fig. 8 A). We also treated mice twice daily with UNC2025 or vehicle for 14 d and monitored blood glucose levels for diabetes. We chose ≥20-wk-old female NOD mice, because we reasoned that this cohort would have a high proportion of infiltrated islets, where MERTK signaling might be driving T cell regulation. Additionally, we treated WT female C57Bl/6 mice with UNC2025 as an additional control to ensure

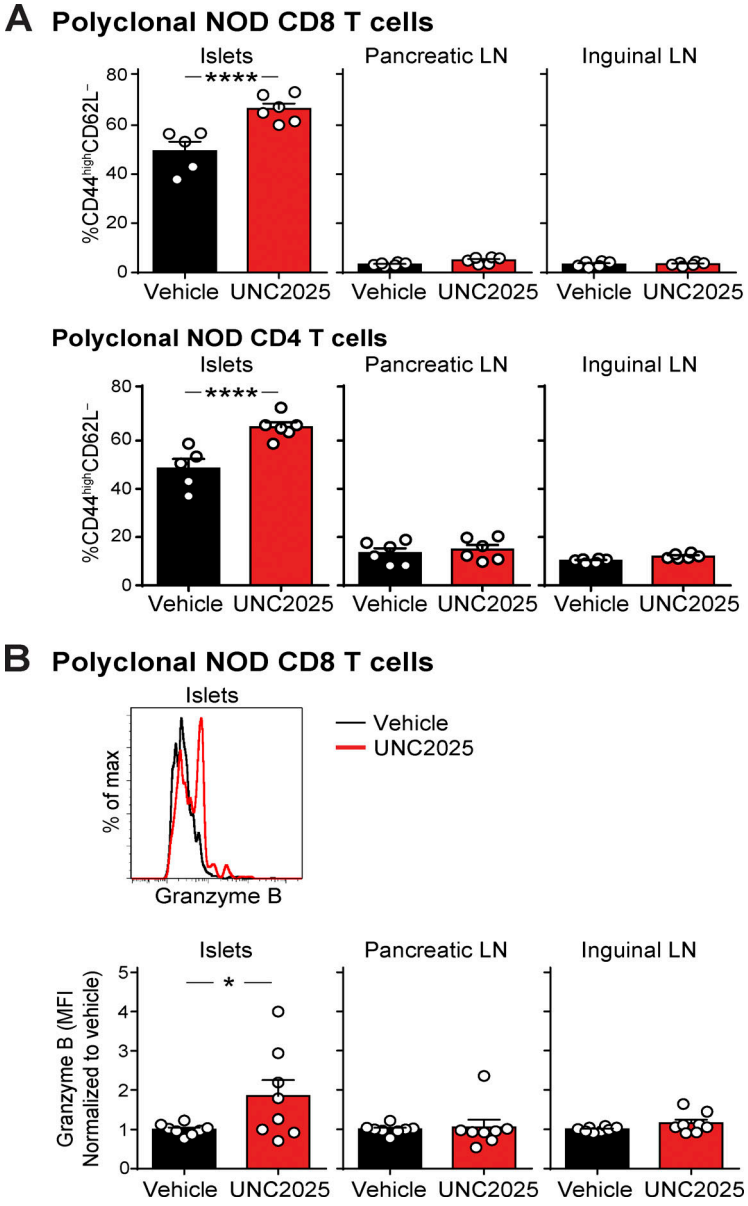

Figure 7. **T cell antigen experience and effector function increases specifically at the disease site in islets following MERTK inhibition. (A and B)** NOD female mice were treated with UNC2025 or vehicle. Islets and LNs were isolated 17 h after treatment initiation, digested, stained and analyzed by flow cytometry. **(A)** Quantification of antigen experience by CD44/CD62L expression. Gated on $CD45^+CD90.2^+CD8^+$ or $CD45^+CD90.2^+CD4^+$. $n = 6$ mice per group from two independent experiments. Statistics: two-way ANOVA with Bonferroni post-test. Error bars represent SEM. **(B)** Quantification of effector function by granzyme B expression. Mice were treated in vivo with Brefeldin A for 4 h before harvest to block secretion. Cells were gated on $CD45^+CD8^+$granzyme B^+. Granzyme B expression was measured by normalized MFI. $n = 8$ mice per group from four independent experiments. Error bars represent SEM. Statistics performed on the nonnormalized MFI values using a Mann–Whitney test. *, $P < 0.05$, ****, $P < 0.0001$.

that UNC2025 did not have direct β cell toxicity. MERTK inhibition by UNC2025 treatment rapidly induced diabetes in a subset of the NOD mice (Fig. 8 B). Diabetes incidence was similar to the incidence of enhanced effector function following MERTK inhibition, suggesting that additional tolerance mechanisms within islets may be protecting some of the mice. The rapid nature of disease onset suggests that MERTK is playing a critical role in regulating T cell pathogenesis in islets to prevent rapid disease progression during T1D. This led us to the question of whether MERTK also functions in human T1D to protect islets from destruction.

Remaining intact islets of T1D patients have increased numbers of MERTK-expressing cells

We hypothesized that if MERTK protects islets during T1D, then we would see an increased number of MERTK-expressing cells in the remaining intact islets of T1D patients. Thus, we used immunofluorescent staining of pancreatic sections from control and T1D donors obtained from nPOD (Network for Pancreatic Organ Donors with Diabetes) to test this hypothesis (Fig. 8, C–E). Control and T1D donors had a similar mean age and sex distribution (control: 23.3–44 yr, mean 34.5 yr; T1D: 20.3–45 yr, mean 33.6 yr; Fig. 8 D and Table S1). The T1D patients had long-standing disease of 10–20 yr (Table S1). Insulin-containing islets from T1D patients showed a significant increase in the number of MERTK-expressing cells in islets when compared with islets of controls (Fig. 8, C and E). Cell numbers per islet were normalized to the average area of all islets analyzed. Co-staining with the macrophage marker CD68 showed increased macrophages and MERTK-expressing macrophages in insulin-containing islets of T1D patients compared with control islets. Not all MERTK-expressing cells in islets expressed CD68, suggesting that other mononuclear phagocyte subsets express MERTK in human islets (Fig. 8, C and E). These data support our hypothesis that MERTK-expressing mononuclear phagocytes could protect human islets from autoimmune destruction.

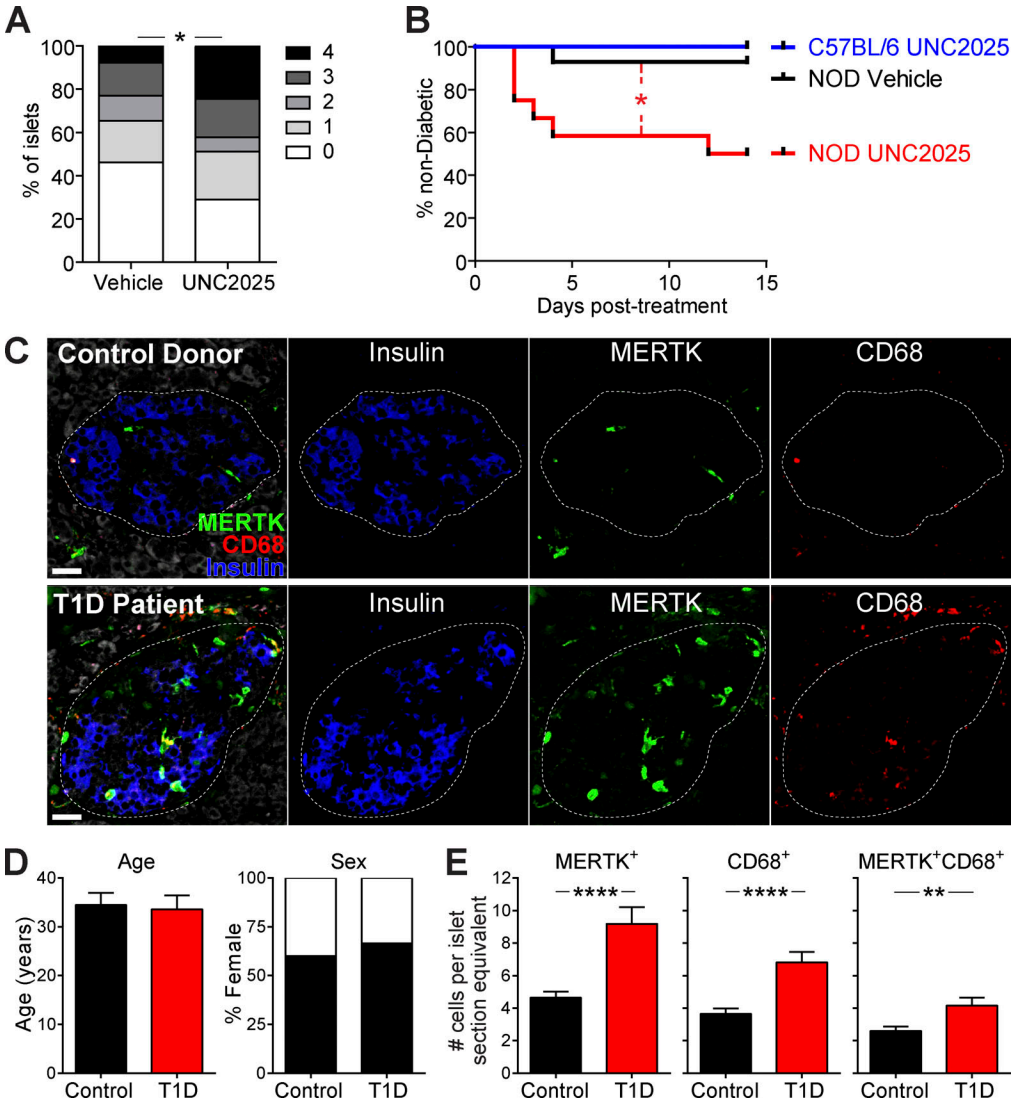

Figure 8. **MERTK signaling prevents rapid T1D progression in mice and MERTK-expressing cells are increased in the remaining insulin-containing islets of T1D patients. (A and B)** NOD female mice >20 wk of age or WT C57BL/6 female mice were treated orally twice daily with 30 mg/kg UNC2025 or saline vehicle twice daily for 16 h (A) or 14 d (B). **(A)** Quantification of islet infiltration following MERTK inhibition. Whole pancreata were isolated and fixed before sectioning and staining. Sections were scored blindly for islet infiltration using the standard insulitis scale of 0 (uninfiltrated islet) to 4 (completely destroyed islet). *n* = 45 islets per condition from five or six mice per group from two independent experiments. Statistics: Student's t test of islet scores. **(B)** Diabetes incidence with MERTK inhibition. Mice were monitored daily for blood glucose values. Mice with two consecutive blood glucose readings of >250 mg/dl were considered to be diabetic. *n* = 6–14 mice per group from four independent experiments. Statistics: Mantel–Cox test. **(C–E)** Immunofluorescent staining of pancreas sections from T1D patient and control donors. **(C)** Representative images of MERTK staining (green), CD68 staining (red), insulin staining (blue), and tissue autofluorescence (white). The dotted line indicates the islet border. Scale bars, 30 µm. **(D)** Donor information. **(E)** Blinded quantification of MERTK-expressing cell number per islet section. *n* = 118 islets from 9 T1D patients and 131 islets from 10 controls. Error bars represent SEM. Statistics: two-tailed Student's t test. *, P < 0.05; **, P < 0.01; ****, P < 0.0001.

Discussion

In this study, we sought to determine the mechanism by which autoreactive T cells are regulated at the tissue site of disease. Our results indicate that following inflammation, CD11c-expressing cells act to prevent T cells from effectively searching for and responding to antigen by promoting rapid T cell scanning of APCs with low-sensitivity antigen detection. This mechanism of T cell regulation is not dependent on classical DCs. Instead, MERTK signaling in macrophages and/or monocytes suppressed local T cell stimulation by preventing T cells from effectively scanning for antigen and responding to antigen-bearing APCs in islets during T1D and at a solid tumor site. Inhibition of this MERTK-mediated mechanism of T cell regulation led to increased antigen experience and effector function by T cells at the autoimmune site, but not in draining LNs. Ultimately, inhibition of MERTK-mediated immune regulation led to the acceleration of autoimmune pathology and disease progression. Increased numbers of MERTK-expressing cells were also observed in the remaining intact islets of T1D patients. Together, these data indicate that MERTK signaling in mononuclear phagocytes drives T cell regulation at the disease site in peripheral tissues. MERTK-mediated regulation is achieved by reducing the

sensitivity of T cell scanning of the local antigenic landscape, thereby suppressing detection of and responsiveness to antigenic stimuli.

Our previous work indicated that T cell stimulation in the autoimmune lesion is controlled by modulating antigen-mediated T cell arrest during disease progression (Friedman et al., 2014; Lindsay et al., 2015). In T1D progression, mild insulitis was characterized by antigen-mediated T cell arrest and restimulation, while advanced insulitis was characterized by the loss of antigen-mediated T cell arrest and antigenic stimulation despite locally presented cognate antigen (Friedman et al., 2014; Lindsay et al., 2015). These data suggest that tolerogenic pathways are functioning to prevent antigen-mediated T cell arrest. In a variety of systems, T cell tolerance induction has been associated with a lack of T cell arrest and transient T cell–APC interactions (Jacobelli et al., 2013). For example, prevention of antigen-mediated T cell arrest as a means of tolerance induction has been established for the PD-1 pathway (Fife et al., 2009), where PD-1 signaling dephosphorylates CD28 to prevent costimulation (Hui et al., 2017). Notably, we have shown that blockade of PD-1 is not sufficient to restore antigen-mediated T cell arrest in advanced insulitis (Friedman et al., 2014) and that PD-L1 expression is not altered by MERTK inhibition (Fig. S4). While MERTK signaling is known to play a role in immune regulation (Wallet et al., 2009; Scott et al., 2001; van der Meer et al., 2014; Cabezón et al., 2015), it has not previously been implicated in suppressing the T cell response by inhibiting effective scanning for antigen and antigen-mediated T cell arrest. Here, we show that inhibition of or deficiency in MERTK leads to increased T cell arrest within T1D islets and at a solid tumor site.

T cell behavior in islets during T1D is controlled by the islet milieu, which is dependent on the disease state of the individual islet (Friedman et al., 2014). Here, we show that MERTK-expressing mononuclear phagocytes are responsible for controlling the T cell response by altering the islet environment. The T cell–extrinsic nature of this process is highlighted by the fact that mouse T cells do not express MERTK and that T cell behavior in islets and tumor were altered in WT T cells within a MERTK-deficient environment. The evidence for MERTK-expressing mononuclear phagocytes driving this effect is particularly strong in the tumor model where both the T cells and tumor carried a WT MERTK gene, and only the host cells recruited to the tumor, including mononuclear phagocytes, were MERTK-deficient.

While MERTK-mediated regulation is T cell extrinsic, there is a possible role for T cells in promoting MERTK signaling in the mononuclear phagocytes. Activated T cells can express the MERTK ligand Protein S, and the T cell derived Protein S can act to restrict the activation of DCs (Carrera Silva et al., 2013). Additionally, viable T cells can expose patches of phosphatidyl serine on their surface upon antigen recognition (Fischer et al., 2006), which could serve together with Protein S as a ligand on T cells to induce MERTK signaling. Thus, while MERTK-mediated regulation is T cell extrinsic, it is possible that T cells contribute to the induction of MERTK signaling. In contrast to mouse T cells, human T cells can express MERTK, which can function as a costimulatory molecule, making the players responsible for MERTK signaling in human settings more complex (Peeters et al., 2019). Further studies will be needed in human disease settings to determine the precise role of MERTK signaling on different cell types.

Polyclonal T cells showed reduced motility in islets following MERTK inhibition, showing that the altered islet milieu induced by MERTK inhibition modifies T cell behavior in an antigen-independent manner. Yet, increased T cell–APC interactions were dependent on antigen specificity, indicating that enhancing T cell scanning increased the T cell's ability to detect local cognate antigen. Patterns of T cell scanning for cognate antigen in target tissues such as pancreatic islets or tumors are controlled by a variety of different cues from the local environment, including ligands for adhesion molecules, physical characteristics of the tissue, chemokines and cytokines, and presented antigen. The balance of these cues alters the efficiency and sensitivity of the T cell search for antigen (Krummel et al., 2016; Fowell and Kim, 2021). Our data suggest that MERTK signaling in mononuclear phagocytes establishes a regulatory milieu that promotes a T cell search pattern that prioritizes high-speed scanning over sensitivity to antigen. We believe that this represents one of the mechanisms by which MERTK signaling functions to reestablish homeostasis following an immune response. While mononuclear phagocytes in the islet environment use MERTK signaling to try to reestablish homeostasis, in T1D, the failure of this pathway enables continued destruction of islets. MERTK signaling in tumor-associated mononuclear phagocytes enables the tumor to escape T cell surveillance by reducing T cell sensitivity to local antigen.

MERTK signaling suppresses the NF-κB pathway (Sen et al., 2007; Zhang et al., 2017; Camenisch et al., 1999). NF-κB target genes include the proinflammatory cytokines TNF-α, IL-1β, IL-6, and IL-12p40 (Liu et al., 2017), which can all be expressed by mononuclear phagocytes and can be suppressed by the MERTK signaling axis (Zhang et al., 2017; Wallet et al., 2008; Camenisch et al., 1999; Maimon et al., 2021). Given the role of the islet milieu in controlling T cell responsiveness in islets (Friedman et al., 2014), this leads us to hypothesize that MERTK signaling creates a regulatory milieu by modulating soluble mediators such as cytokines that alter T cell scanning by tuning T cell adhesion and responsiveness to antigen.

Many mechanisms work in concert to maintain and restore self-tolerance. This might be in part why MERTK inhibition led to increased effector function and disease progression in only half of the mice treated. It is likely that other mechanisms of tolerance were able to compensate for MERTK in some of the subjects, preventing the increased effector function and islet destruction. Despite preventing increased effector functions, other tolerance mechanisms were unable to prevent restoration of T cell arrest in both islets and tumor. The asynchronous nature of disease in the NOD model might also play into this dichotomy, since our data suggest that MERTK is functioning specifically within infiltrated islets. Thus, the percentage of uninfiltrated islets, which will not be destroyed upon MERTK inhibition, might determine whether or not MERTK inhibition results in overt diabetes. Coinhibitory molecules such as CTLA-4,

PD-1, and LAG-3 (Ansari et al., 2003; Keir et al., 2006; Bettini et al., 2011; Lühder et al., 1998; Luhder et al., 2000), as well as regulatory T cells, also provide layers of tolerance in the progression of T1D (Tang et al., 2004a; Tarbell et al., 2007; Tonkin and Haskins, 2009). These regulatory mechanisms have roles both in the draining LN and at the disease site (Tang et al., 2004b; Bettini et al., 2011; Keir et al., 2006; Fife et al., 2009; Lühder et al., 1998; Luhder et al., 2000; Tarbell et al., 2007; Tonkin and Haskins, 2009). The role of MERTK in driving T cell tolerance following well-established inflammation at the disease site could make it of particular importance when considering mechanisms that are critical in targeting tolerance of established disease at the site of pathology.

T1D has been proposed to be a relapsing remitting disease (von Herrath et al., 2007; van Megen et al., 2017); thus, the temporal regulation of T cell pathogenesis in islets could represent relapsing and remitting phases of disease within individual islets. Cycles of MERTK signaling initiation in the presence of β cell apoptosis followed by cessation once the autoimmune β cell destruction is controlled could control cycles of quiescent T cell tolerance followed by destructive reinitiation of T cell pathogenesis.

In this study, we identified MERTK signaling as a key mechanism in driving T cell regulation within pancreatic islets during T1D and at the tumor site. It is known that MERTK deficiency can also result in a systemic, lupus-like autoimmune phenotype (Scott et al., 2001). Furthermore, we would posit that this pathway is likely to inhibit antigen-mediated T cell arrest and stimulation in peripheral tissues under many inflammatory conditions, including other types of tissue-specific autoimmunity and in other solid tumors. In fact, MERTK expression in tumor-infiltrating macrophages has been implicated in enabling tumor growth and metastasis in MMTV-PyVmT and B16:F10 tumor models (Cook et al., 2013). Antibody blockade of MERTK signaling was also recently shown to enhance T cell function in tumors by increasing type I IFN production by macrophages (Zhou et al., 2020). In future studies, it will be important to understand the breadth of function of this MERTK-dependent tolerance pathway, why it fails in autoimmune settings, how it controls the sensitivity of T cell scanning for antigen, and how it inhibits T cell responsiveness to antigen.

Materials and methods

Mice

NOD/ShiLtJ (001976), NOD.8.3 (005868), NOD.CD11c-YFP (009422), C57BL/6.RIP-mOva (005431), C57BL/6.OT-I (003831), C57BL/6.ZBTB46-DTR (019506), C57BL/6.Ubiquitin-GFP (004353), and C57BL/6.MERTK$^{-/-}$ (011122) mice were obtained from The Jackson Laboratory and bred in-house. NOD.BDC-2.5 TCR transgenic (Katz et al., 1993) were a generous gift from the laboratory of Kathryn Haskins, University of Colorado, Anschutz Medical Campus, Aurora, CO. NOD.CD11c-DTR (Saxena et al., 2007) mice were a generous gift from the laboratory of Jonathan Katz, Cincinnati Children's Hospital, Cincinnati, OH. NOD.CD2-dsRed mice were a generous gift from the laboratory of Qizhi Tang, University of California, San Francisco, San Francisco, CA. NOD.MERTK$^{-/-}$ mice were a generous gift from the laboratory of Roland Tisch, University of North Carolina, Chapel Hill, NC. NOD.CX3CR1-GFP mice were generated by backcrossing and were confirmed to be fully backcrossed to our in-house NOD mice using speed congenic analysis performed by the Barbara Davis Center core facilities. All NOD transgenics and knockouts were backcrossed to NOD/ShiLtJ for at least 10 generations. All animal procedures were approved by the Institutional Animal Care and Use Committee at National Jewish Health and University of Colorado Anschutz Medical Campus.

Islet isolation

Islets were isolated as previously described (Melli et al., 2009; Friedman et al., 2014). Briefly, mice were anesthetized with ketamine/xylazine before cervical dislocation. The pancreas was inflated via the common bile duct by adding ∼3 ml of 0.8 mg/ml Collagenase P (Roche) and 10 µg/ml DNase I (Roche) or CIzyme RI (Vitacyte) in HBSS (Cellgro). Following inflation, the pancreas was removed and incubated at 37°C for 10–11 min for collagenase P digestion or 17 min for CIzyme RI digestion, and islets were isolated by density centrifugation. Islets were handpicked under a dissecting microscope. For experiments in which islets were analyzed using flow cytometry, single-cell suspensions were generated by digestion with 0.4 Wunsch units/ml Collagenase D (Roche) and 250 µg/ml DNase I (Roche) in HBSS (Cellgro) with 10% FBS (Hyclone) at 37°C for 30 min. Following initial digestion, islets were then incubated in Cell Dissociation Buffer (Sigma-Aldrich) at 37°C for an additional 30 min.

Tumor implantation and excision

10^5 B78ChOva tumor cells (generous gift of Max Krummel, University of California, San Francisco, San Francisco, CA) were resuspended in PBS and mixed 1:1 with growth factor–reduced Matrigel (Corning). Tumor cells were injected subcutaneously into each flank of WT or MERTK$^{-/-}$ C57BL/6 mice. At the time of harvest, tumors were carefully exposed by peeling the skin away from the peritoneum and excised with a border around the tumor. The skin associated with the tumor was affixed to a coverslip using VetBond (3M).

Two-photon imaging of explanted islets and tumors

For two-photon imaging, isolated islets were embedded in 3% low-melting-temperature agarose (Thermo Fisher Scientific) in DPBS. During imaging, islets and tumors were maintained at 35–37°C with flow of 95% O_2/5% CO_2–saturated RPMI (Gibco). Islets and tumors were imaged on an Olympus FV100MPE microscope or a Leica SP8 DIVE upright multiphoton microscope as previously described (Friedman et al., 2014; Lindsay et al., 2015). Excitation was performed at 810 nm for islets and 910 nm for tumors. Imaging fields were as described previously (McKee et al., 2013), and xy planes of 509 µm by 509 µm with a resolution of 0.994 µm/pixel or xy planes of 592 µm by 592 µm with a resolution of 1.16 µm/pixel were acquired. Images of 27–60 xy planes with 3-µm z-spacing were acquired every minute for 30 min. Four emission channels were used for data acquisition: blue (450–490 nm), green (500–550 nm), red (575–640 nm), and far red (645–685nm). In tumors, collagen was imaged in the blue

channel through second harmonic generation. The collagen was confirmed to be at the surface of the tumor by visualization of the mCherry tumor fluorescence at 810 nm.

Image analysis

Image analysis was performed using Imaris (Bitplane) and MATLAB (MathWorks). Images were linearly unmixed, as previously described (Bullen et al., 2009). Islet infiltration levels were determined as previous described (Lindsay et al., 2015). Islets with similar levels of infiltration between groups were used for comparison. Cells in islets that could be tracked for ≥5 min were used to obtain speed and average arrest coefficient (<1.5 µm/min cutoff for islets due to overall lower T cell speeds in islets; <2 µm/min cutoff for tumors). Cells tracked for ≥10 min in islets were used to determine MSD to ensure all cells analyzed could be included for all time points of the analysis. Interaction duration was calculated using a maximum distance between cells of 1 pixel (1.16 µm), with a minimum interaction of two time points to be defined as an interaction. Sustained interactions were defined as ≥10-min-long interactions. Statistics were calculated with Prism software (GraphPad).

Activation and dye labeling of BD2.5, 8.3, polyclonal NOD, and OT-I T cells

Spleen and LN cells from female BDC-2.5 or 8.3 mice or male/female OT-I.Ubiquitin-GFP mice were stimulated in vitro with 1 µg/ml BDC-2.5 mimetope (YVRPLWVRME; Pi Proteomics), 1 µg/ml 8.3 peptide (KYNKANVEL; Chi Scientific), or 100 ng/ml of OT-I peptide (SIINFEKL; Pi Proteomics). Spleen and LN cells from 8-wk-old female NOD mice were stimulated with soluble 2 µg/ml anti-CD28 antibody (BioXCell) and plate-bound 2 µg/ml anti-CD3 antibody (BioXCell). Beginning on day 2 after activation, cells were maintained in media containing 10 IU/ml rhIL-2 (AIDS Research and Reference Reagent Program, Division of AIDS, National Institute of Allergy and Infectious Diseases, National Institutes of Health from Dr. Maurice Gately; Hoffman-La Roche). Days 6–9 after activation, BDC2.5 or 8.3 T cells were labeled with 1 µM Violet Proliferation Dye (VPD; BD), 2 µM CFSE (Invitrogen), 20 µM CellTracker Orange (CMTMR; Invitrogen), or 5 µM eFluor670 (eBiosciences) for 25–30 min at 37°C or 0.5 µM CellTrace Far Red (Thermo Fisher Scientific) or 2.5 µM CellTrace Yellow (Thermo Fisher Scientific) for 15 min at 37°C. 10^7 T cells were transferred intravenously into recipients with the timing indicated in the schematics provided for each experiment.

Generation and treatment of BM chimeras

CD11c-DTR mixed BM chimeras

8-wk-old WT NOD female mice were lethally γ-irradiated with two doses of 500 Rads. Following irradiation, 10^7 BM cells (90% NOD.CD11c-DTR and 10% NOD.8.3.CD2-dsRed.CD11c-DTR or 95% NOD.CD11c-DTR and 5% NOD.CD11c-DTR.CD2-dsRed) were injected intravenously via the tail. BM chimeras were allowed to reconstitute for at least 8 wk before use. Following reconstitution mice were injected with two doses of 200 ng DT (Sigma-Aldrich) or control PBS 24 h apart. 24 h after the final DT treatment, islets were isolated and mounted for two-photon imaging.

ZBTB46-DTR BM chimeras

C57BL/6.RIP-mOva mice were γ-irradiated with two doses of 500 Rads. Following irradiation, 10^7 C57BL/6.ZBTB-46-DTR BM cells were injected intravenously via the tail. BM chimeras were allowed to reconstitute for at least 8 wk before use. C57BL/6.OT-I.Ubiquitin-GFP $CD8^+$ T cells were enriched from single-cell suspensions of LNs and spleens using mouse CD8-negative selection kits (Stem Cell Technologies). Enriched CD8 T cells (5×10^6) were injected into ZBTB-46-DTR-RIP-mOva BM chimeras to induce islet infiltration. 2 d before islet isolation, mice were treated with two doses of 200 ng DT or control PBS 24 h apart to deplete ZBTB-46 expressing cells. Day 5–7 after T cell transfer, islets were isolated for explanted imaging. Following islet isolation, T cell motility was assessed as by two-photon imaging.

Flow cytometry: Tissue preparation and antibodies

Tissue isolation and digestion

Islets were isolated and digested as described above. PLNs (draining) or ILNs (nondraining) were isolated and shredded using needles. LNs were then digested with 0.4 Wunsch units/ml Collagenase D (Roche) and 250 µg/ml DNase I (Roche) in HBSS (Cellgro) with 10% FBS (Hyclone) at 37°C for 30 min.

MERTK identification panel

Islets were isolated from 4–18-wk-old NOD.CX3CR1-$GFP^{+/-}$ mice and dissociated as previously described. Islet samples were stained with the fluorescent-labeled antibodies CD11c PE-Cy7 (BioLegend), MHC-II PE (BioLegend), CD45 Pacific Blue (BioLegend), unlabeled goat α-MERTK (R&D Systems), and donkey α-goat secondary (AF647; Jackson ImmunoResearch).

T cell activation panel

Isolated islet and LN cells were surface stained with CD45 BUV395 (BD), CD4 BV711 (BioLegend), CD8 APC-780 (eBioscience), CD62L Pacific Blue (BioLegend), and CD44 FITC (BioLegend) for 30 min on ice.

Granzyme B intracellular panel

Isolated islet and LN cells were stained with the fluorescent antibodies CD45 BUV395 (BD), CD4 BV711 (BioLegend), CD8 FITC (BioLegend), dump PerCP-cy5.5 (CD11c; eBioscience), CD11b (BioLegend), Ter119 (BD), F4/80 (BioLegend), and CD19 (BD) on ice for 30 min. Following surface staining, samples were fixed with 1% PFA (Sigma-Aldrich) and 3% sucrose (Sigma-Aldrich) for 13 min. Following fixation samples were stored overnight in permeabilization buffer (eBioscience). After overnight permeabilization, samples were stained intracellularly with granzyme B (Pacific Blue; BioLegend) for 30 min at room temperature.

APC identification panel

Islets were isolated from ZBTB46-DTR BM chimera mice dissociated as previously described. Islet samples were stained with the fluorescent-labeled antibodies CD45 BUV395 (BD), CD90.2 PE-Cy7 (BioLegend), CD19 PE (BioLegend), F4/80 PerCP-Cy5.5 (BioLegend), MHC-II FITC (BioLegend), CD11c BUV805

(BD), CD11b APC-Cy7 (BioLegend), XCR1 BV785 (BioLegend), unlabeled goat α-MERTK (R&D Systems), and donkey α-goat secondary (AF647; Jackson ImmunoResearch).

MERTK identification in CD11c-DTR-GFP mice

Islets were isolated from NOD.CD11c-DTR-GFP mice as previously described. Islet samples were stained with the fluorescent-labeled antibodies CD45 BUV395 (BD), CD90.2 BUV737 (BD), CD19 BUV737 (BD), CD11c PE-Cy7, CD11b Alexa Fluor 647, XCR1 BV785, MHC-II Biotin (BD), Streptavidin Qdot605 (Invitrogen), rabbit α-MERTK (Abcam), and donkey α-rabbit BV421 (BioLegend).

Flow cytometry and analysis

All samples were run on an LSR Fortessa (BD) or Aurora (Cytek). Analysis and conventional compensation were performed in FlowJo (Tree Star). Spectral unmixing was performed using or SpectroFlo (Cytek).

In vivo treatment with UNC2025

UNC2025 is a selective MERTK/Flt3 kinase inhibitor (Zhang et al., 2014) that was initially developed to inhibit MERTK signaling in MERTK$^+$ leukemia cells (Zhang et al., 2014; DeRyckere et al., 2017). UNC2025 is orally bioavailable; however, it has a short half-life that requires twice-daily dosing. UNC2025 (Meryx) was dosed at 30 mg/kg, which has been used to treat mice in a cancer setting (Cook et al., 2013; Cummings et al., 2015). Mice were treated twice daily for up to 4 wk as indicated with daily monitoring of blood glucose and body weight.

Diabetes incidence

For disease incidence experiments, all mice had normal glycemia before treatment. Blood glucose readings were taken daily before afternoon treatment. Mice with two consecutive readings >250 mg/dl were considered diabetic and euthanized. Mice were treated for at least 2 wk unless sacrificed due to diabetes.

T cell activation

WT NOD 12–16-wk-old female mice were treated with 30 mg/kg UNC2025 or vehicle. 16 h later, mice were treated a second time with UNC2025 or vehicle. 1 h after the final treatment, islets, draining PLNs, and nondraining ILNs were harvested and digested as described above. Single-cell suspensions were labeled with the T cell activation panel described above.

In vivo granzyme B

WT NOD 12–16-wk-old female mice were treated for 16 h with UNC2025 or vehicle in the same manner as described above. At the same time as the final UNC2025 treatment, mice were injected intravenously with 250 µg Brefeldin A (Sigma-Aldrich). 4 h after Brefeldin A injection, islets, draining PLNs, and nondraining ILNs were harvested. Samples were maintained in 10 µg/ml Brefeldin A on ice when possible until fixation. Islets and LNs were digested and dissociated as described above. Staining was performed using the Granzyme B panel as described above. Due to changes in cytometer settings between experiments, mean fluorescent intensity (MFI) data were normalized for the purposes of graphing all experiments together. All samples were normalized to the average value of the vehicle controls from the same tissue in the same experiment. However, statistical analysis was performed on the data before normalization.

Islet section scoring

WT NOD female mice >20 wk of age were treated twice daily with 30 mg/kg UNC2025 or vehicle. For islet sections, mice were treated twice 16 h apart with UNC2025 or vehicle. 1 h after the final treatment, the whole pancreas was excised and fixed in formalin (VWR) for 4 d. After fixation, samples were stored in 70% ethanol until embedding in paraffin. 7-µm sections were cut and fixed with hematoxylin and eosin. Embedding, sectioning, and staining were performed by the University of Colorado Denver Anschutz histology core. Section scoring was performed blindly on a scale of 0 (no infiltration) to 4 (completely infiltrated).

Formalin-fixed paraffin-embedded human pancreas sections were obtained from nPOD. Sections were deparaffinized using mixed xylenes (Sigma-Aldrich), and antigen retrieval was done using Tris pH 10 antigen retrieval buffer in a pressure cooker for 10 min. Islets were stained for insulin (polyclonal guinea pig), CD3 (clone CD3-12), MERTK (clone Y323), and CD68 (clone KP1), all from Abcam. Secondaries included anti-GP-Cy3, anti-rat-DL649, anti-mouse-biotin, anti-rabbit-biotin (all donkey antibodies from Jackson ImmunoResearch), Streptavidin-FITC, and Streptavidin-BV421 (BioLegend). MERTK and CD68 stains were done sequentially with biotin-avidin blocking (Life Technologies) between stains. Differential staining patterns for CD68 and MERTK confirmed successful blocking. Approximately 10 insulin-containing islets were imaged per donor using a Zeiss 710 confocal microscope. Islet images were analyzed in a blinded manner using Imaris software.

Analysis of UNC2025 treatment by imaging

Activated BDC-2.5, 8.3, and Polyclonal T cells were labeled with VPD, CellTrace Far Red, or CellTrace Yellow and transferred intravenously into 12–16-wk-old NOD.CD11c-YFP female mice. 8 h following T cell transfer, mice were treated with 30 mg/kg UNC2025 or vehicle. 16 h later, mice were again treated with UNC2025 or vehicle. 1 h later, islets were isolated and imaged using our explanted imaging technique as previously described (explanted islet imaging).

Activated OT-I.Ubiquitin-GFP T cells were transferred into WT or MERTK$^{-/-}$ tumor–bearing hosts 5–7 d before treatment. 18 h before tumor harvest, mice were treated with 30 mg/kg UNC2025 or vehicle by oral gavage. Whole tumors were excised and mounted on coverslips for imaging. To ensure comparable microenvironments, tumor imaging was done in superficial regions of the tumor, where OT-I T cells were present and the collagen-rich tumor capsule was visible.

UNC2025-treated tumor explants were maintained in 50 µM UNC2025 and islet explants were maintained in 30 µM UNC202 for the duration of isolation and imaging. Imaging duration was 30 min; image analysis was performed using Imaris and MATLAB as previously described.

Analysis of T cell motility within MERTK$^{-/-}$ islets

For studies involving NOD.MERTK$^{-/-}$ mice, which do not spontaneously develop diabetes, islet infiltration was induced in NOD.MERTK$^{-/-}$ or control WT mice by transferring 10^7 activated BDC-2.5 T cells 3–6 d before dye-labeled T cell transfer. Following initiation of islet infiltration, 10^7 VPD or eFlour670 dye–labeled activated BDC2.5 and 8.3 T cells were transferred intravenously. 24 h following labeled T cell transfer, islets were isolated and imaged by two-photon microscopy. Imaging duration was 30 min; image analysis was performed using Imaris and MATLAB as previously described.

Immunofluorescent staining and analysis of human islets

Deidentified formalin-fixed paraffin-embedded pancreas sections were obtained from the nPOD consortium. The experiments were determined to be nonhuman subject research by the National Jewish Health Institutional Review Board. Donor information is noted in Table S1. Sections were deparaffinized with xylene, and antigen retrieval was performed with Tris pH 10 buffer in a pressure cooker. Sections were blocked with 10% donkey serum (Jackson ImmunoResearch) and a biotin-avidin blocking kit (Thermo Fisher Scientific). Pancreas sections were then stained for insulin, MERTK, CD68, and CD3 (ab955, ab52968, ab7842, and ab11089; Abcam). Anti-insulin and anti-CD3 were detected with fluorescently labeled secondary antibodies (706–166-148 and 712–606-153; Jackson ImmunoResearch). CD68 was detected using a biotin-conjugated secondary antibody (715–065-151; Jackson ImmunoResearch) followed by fluorescently conjugated streptavidin (405201; BioLegend). The avidin-biotin blocking kit was then used to block any free streptavidin and biotin. After blocking of CD68–biotin–avidin was complete, MERTK was then detected using a biotin-conjugated secondary antibody (711–065-152; Jackson ImmunoResearch) followed by fluorescently conjugated streptavidin (405226; BioLegend). Data were acquired using a Zeiss LSM700 microscope. 10 pancreas images from each donor were acquired based on expression of insulin.

Samples were blinded before analysis and analysis was performed by a third party. 10–15 islets per donor were analyzed, with an average of 13.10 islets per control donor and 13.11 islets per T1D donor analyzed. Image visualization and determination of islet area were performed using Imaris (Oxford Instruments).

Online supplemental material

Fig. S1 shows that the CD11c-DTR-GFP cells are effectively depleted in islets upon DT treatment and that islet CD11c-DTR-GFP cells include CD11b$^+$, XCR1$^+$, and MERTK$^+$ populations. Fig. S2 shows that Zbtb46-expressing DCs are not the subset of CD11c$^+$ cells in islets that prevent T cell arrest. Fig. S3 shows that MERTK deficiency or MERTK inhibition do not alter the mononuclear phagocyte frequency in islets. Fig. S4 shows that costimulatory and coinhibitory molecule expression on CD11c$^+$ cells is not altered by MERTK inhibition. Fig. S5 shows examples of CD44/CD62L flow cytometry gating. Video 1 is an example of the data analyzed in Fig. 1, which shows that T cell motility in islets is reduced upon CD11c$^+$ cell depletion. Video 2 is an example of the data analyzed in Fig. 3, which shows that T cell motility is reduced in MERTK-deficient islets. Video 3 is an example of the data analyzed in Fig. 5, which shows that T cell motility on the surface of a melanoma tumor is reduced with either MERTK inhibition or MERTK deficiency in the tumor host. Video 4 is an example of the data analyzed in Figs. 4 and 6, which show that in islets, sustained interactions between islet-antigen–specific T cells and CD11c$^+$ cells are increased with MERTK inhibition, while T cells that are not specific for islet-antigen show no change in T cell–CD11c$^+$ cell interactions. Table S1 displays information about the donor samples analyzed in Fig. 8.

Acknowledgments

We thank Meryx for providing UNC2025; Dr. Jonathan Katz, Dr. Katie Haskins, Dr. Qizhi Tang, and Dr. Roland Tisch for mice; Dr. Katie Haskins, Dr. John Cambier, Dr. Michael Holers, Dr. Ron Gill, Dr. Claudia Jakubzick, Dr. Ross Kedl, Dr. Rocky Baker, Dr. Mira Estin, and Dr. Scott Thompson for guidance and helpful scientific input; Dr. Pippa Marrack, Dr. John Kappler, Dr. Ross Kedl, Dr. Claudia Jakubzick, Dr. Larry Wysocki, and Dr. Laurel Lenz for reagents; Robert Long, Matthew Gebert, Brianna Traxinger, Marlie Fisher, Katie Morgan, and Jessica Olivas, Scott Beard, the National Jewish Health Flow Cytometry Core Facility, the National Jewish Health Biological Resource Center, the Barbara Davis Center Flow Cytometry Core, and University of Colorado Vivarium for animal husbandry and technical assistance; Bonnie Levitt and Joseph Kleponis for assistance with coding MATLAB analysis scripts.

This research was performed with the support of nPOD (RRID:SCR_014641), a collaborative T1D research project sponsored by the Juvenile Diabetes Research Foundation (nPOD; 5-SRA-2018-557-Q-R), and the Leona M. and Harry B. Helmsley Charitable Trust (grant 2018PG-T1D053). Organ procurement organizations partnering with nPOD to provide research resources are listed at http://www.jdrfnpod.org//for-partners/npod-partners/. This work was supported by funding from Juvenile Diabetes Research Foundation grant 2-2012-197 (R.S. Friedman), the William and Ella Owens Medical Research Foundation (R.S. Friedman), National Institutes of Health grant 1R01DK111733-01 (R.S. Friedman), the Juvenile Diabetes Research Foundation/Leona M. and Harry B. Helmsley Charitable Trust George S. Eisenbarth nPOD Award (R.S. Friedman), Cancer Research Institute #AWD-112499 (to support R.S. Lindsay), National Institutes of Health grant T32: 5T32AI007405-27 (to support J.C. Whitesell), and the University of Colorado Diabetes Research Center (National Institutes of Health grant P30-DK116073).

Author contributions: conceptualization, R.S. Friedman and R.S. Lindsay; methodology, R.S. Friedman, R.S. Lindsay, J.C. Whitesell, and J. Jacobelli; investigation, R.S. Lindsay, J.C. Whitesell, K.E. Dew, E. Rodriguez, A.M. Sandor, D. Tracy, S.F. Yannacone, B.N. Basta, and R.S. Friedman; analysis, R.S. Lindsay, R.S. Friedman, J.C. Whitesell, E. Rodriguez, B.N. Basta, and J. Jacobelli; writing – original draft, R.S. Friedman and R.S. Lindsay; writing – review & editing, R.S. Friedman, R.S. Lindsay, J.C. Whitesell, A.M. Sandor, and J. Jacobelli; funding acquisition, R.S. Friedman; supervision, R.S. Friedman.

Disclosures: The authors declare no competing interests exist.

Submitted: 10 March 2020
Revised: 4 June 2021
Accepted: 26 July 2021

References

Akalu, Y.T., C.V. Rothlin, and S. Ghosh. 2017. TAM receptor tyrosine kinases as emerging targets of innate immune checkpoint blockade for cancer therapy. *Immunol. Rev.* 276:165–177. https://doi.org/10.1111/imr.12522

Ansari, M.J.I., A.D. Salama, T. Chitnis, R.N. Smith, H. Yagita, H. Akiba, T. Yamazaki, M. Azuma, H. Iwai, S.J. Khoury, et al. 2003. The programmed death-1 (PD-1) pathway regulates autoimmune diabetes in nonobese diabetic (NOD) mice. *J. Exp. Med.* 198:63–69. https://doi.org/10.1084/jem.20022125

Bettini, M., A.L. Szymczak-Workman, K. Forbes, A.H. Castellaw, M. Selby, X. Pan, C.G. Drake, A.J. Korman, and D.A.A. Vignali. 2011. Cutting edge: accelerated autoimmune diabetes in the absence of LAG-3. *J. Immunol.* 187:3493–3498. https://doi.org/10.4049/jimmunol.1100714

Broz, M.L., M. Binnewies, B. Boldajipour, A.E. Nelson, J.L. Pollack, D.J. Erle, A. Barczak, M.D. Rosenblum, A. Daud, D.L. Barber, et al. 2014. Dissecting the tumor myeloid compartment reveals rare activating antigen-presenting cells critical for T cell immunity. *Cancer Cell.* 26:638–652. https://doi.org/10.1016/j.ccell.2014.09.007

Bullen, A., R.S. Friedman, and M.F. Krummel. 2009. Two-photon imaging of the immune system: a custom technology platform for high-speed, multicolor tissue imaging of immune responses. *Curr. Top. Microbiol. Immunol.* 334:1–29. https://doi.org/10.1007/978-3-540-93864-4_1

Cabezón, R., E.A. Carrera-Silva, G. Flórez-Grau, A.E. Errasti, E. Calderón-Gómez, J.J. Lozano, C. España, E. Ricart, J. Panés, C.V. Rothlin, and D. Benítez-Ribas. 2015. MERTK as negative regulator of human T cell activation. *J. Leukoc. Biol.* 97:751–760. https://doi.org/10.1189/jlb.3A0714-334R

Cai, B., C. Kasikara, A.C. Doran, R. Ramakrishnan, R.B. Birge, and I. Tabas. 2018. MerTK signaling in macrophages promotes the synthesis of inflammation resolution mediators by suppressing CaMKII activity. *Sci. Signal.* 11:eaar3721. https://doi.org/10.1126/scisignal.aar3721

Calderon, B., J.A. Carrero, S.T. Ferris, D.K. Sojka, L. Moore, S. Epelman, K.M. Murphy, W.M. Yokoyama, G.J. Randolph, and E.R. Unanue. 2015. The pancreas anatomy conditions the origin and properties of resident macrophages. *J. Exp. Med.* 212:1497–1512. https://doi.org/10.1084/jem.20150496

Camenisch, T.D., B.H. Koller, H.S. Earp, and G.K. Matsushima. 1999. A novel receptor tyrosine kinase, Mer, inhibits TNF-alpha production and lipopolysaccharide-induced endotoxic shock. *J. Immunol.* 162:3498–3503.

Carrera Silva, E.A., P.Y. Chan, L. Joannas, A.E. Errasti, N. Gagliani, L. Bosurgi, M. Jabbour, A. Perry, F. Smith-Chakmakova, D. Mucida, et al. 2013. T cell-derived protein S engages TAM receptor signaling in dendritic cells to control the magnitude of the immune response. *Immunity.* 39:160–170. https://doi.org/10.1016/j.immuni.2013.06.010

Cook, R.S., K.M. Jacobsen, A.M. Wofford, D. DeRyckere, J. Stanford, A.L. Prieto, E. Redente, M. Sandahl, D.M. Hunter, K.E. Strunk, et al. 2013. MerTK inhibition in tumor leukocytes decreases tumor growth and metastasis. *J. Clin. Invest.* 123:3231–3242. https://doi.org/10.1172/JCI67655

Cummings, C.T., W. Zhang, K.D. Davies, G.D. Kirkpatrick, D. Zhang, D. DeRyckere, X. Wang, S.V. Frye, H.S. Earp, and D.K. Graham. 2015. Small molecule inhibition of MERTK is efficacious in non-small cell lung cancer models independent of driver oncogene status. *Mol. Cancer Ther.* 14:2014–2022. https://doi.org/10.1158/1535-7163.MCT-15-0116

DeRyckere, D., A.B. Lee-Sherick, M.G. Huey, A.A. Hill, J.W. Tyner, K.M. Jacobsen, L.S. Page, G.G. Kirkpatrick, F. Eryildiz, S.A. Montgomery, et al. 2017. UNC2025, a MERTK small-molecule inhibitor, is therapeutically effective alone and in combination with methotrexate in leukemia models. *Clin. Cancer Res.* 23:1481–1492. https://doi.org/10.1158/1078-0432.CCR-16-1330

Ferris, S.T., J.A. Carrero, J.F. Mohan, B. Calderon, K.M. Murphy, and E.R. Unanue. 2014. A minor subset of Batf3-dependent antigen-presenting cells in islets of Langerhans is essential for the development of autoimmune diabetes. *Immunity.* 41:657–669. https://doi.org/10.1016/j.immuni.2014.09.012

Fife, B.T., K.E. Pauken, T.N. Eagar, T. Obu, J. Wu, Q. Tang, M. Azuma, M.F. Krummel, and J.A. Bluestone. 2009. Interactions between PD-1 and PD-L1 promote tolerance by blocking the TCR-induced stop signal. *Nat. Immunol.* 10:1185–1192. https://doi.org/10.1038/ni.1790

Fischer, K., S. Voelkl, J. Berger, R. Andreesen, T. Pomorski, and A. Mackensen. 2006. Antigen recognition induces phosphatidylserine exposure on the cell surface of human CD8$^+$ T cells. *Blood.* 108:4094–4101. https://doi.org/10.1182/blood-2006-03-011742

Fowell, D.J., and M. Kim. 2021. The spatio-temporal control of effector T cell migration. *Nat. Rev. Immunol.* https://doi.org/10.1038/s41577-021-00507-0

Friedman, R.S., R.S. Lindsay, J.K. Lilly, V. Nguyen, C.M. Sorensen, J. Jacobelli, and M.F. Krummel. 2014. An evolving autoimmune microenvironment regulates the quality of effector T cell restimulation and function. *Proc. Natl. Acad. Sci. USA.* 111:9223–9228. https://doi.org/10.1073/pnas.1322193111

Gagnerault, M.-C., J.J. Luan, C. Lotton, and F. Lepault. 2002. Pancreatic lymph nodes are required for priming of beta cell reactive T cells in NOD mice. *J. Exp. Med.* 196:369–377. https://doi.org/10.1084/jem.20011353

Guilliams, M., F. Ginhoux, C. Jakubzick, S.H. Naik, N. Onai, B.U. Schraml, E. Segura, R. Tussiwand, and S. Yona. 2014. Dendritic cells, monocytes and macrophages: a unified nomenclature based on ontogeny. *Nat. Rev. Immunol.* 14:571–578. https://doi.org/10.1038/nri3712

Hodi, F.S., S.J. O'Day, D.F. McDermott, R.W. Weber, J.A. Sosman, J.B. Haanen, R. Gonzalez, C. Robert, D. Schadendorf, J.C. Hassel, et al. 2010. Improved survival with ipilimumab in patients with metastatic melanoma. *N. Engl. J. Med.* 363:711–723. https://doi.org/10.1056/NEJMoa1003466

Hugues, S., L. Fetler, L. Bonifaz, J. Helft, F. Amblard, and S. Amigorena. 2004. Distinct T cell dynamics in lymph nodes during the induction of tolerance and immunity. *Nat. Immunol.* 5:1235–1242. https://doi.org/10.1038/ni1134

Hui, E., J. Cheung, J. Zhu, X. Su, M.J. Taylor, H.A. Wallweber, D.K. Sasmal, J. Huang, J.M. Kim, I. Mellman, and R.D. Vale. 2017. T cell costimulatory receptor CD28 is a primary target for PD-1-mediated inhibition. *Science.* 355:1428–1433. https://doi.org/10.1126/science.aaf1292

Jacobelli, J., R.S. Lindsay, and R.S. Friedman. 2013. Peripheral tolerance and autoimmunity: lessons from in vivo imaging. *Immunol. Res.* 55:146–154. https://doi.org/10.1007/s12026-012-8358-7

Jansen, A., F. Homo-Delarche, H. Hooijkaas, P.J. Leenen, M. Dardenne, and H.A. Drexhage. 1994. Immunohistochemical characterization of monocytes-macrophages and dendritic cells involved in the initiation of the insulitis and beta-cell destruction in NOD mice. *Diabetes.* 43:667–675. https://doi.org/10.2337/diab.43.5.667

Kasikara, C., V. Davra, D. Calianese, K. Geng, T.E. Spires, M. Quigley, M. Wichroski, G. Sriram, L. Suarez-Lopez, M.B. Yaffe, et al. 2019. Pan-TAM tyrosine kinase inhibitor BMS-777607 enhances anti-PD-1 mAb efficacy in a murine model of triple-negative breast cancer. *Cancer Res.* 79:2669–2683. https://doi.org/10.1158/0008-5472.CAN-18-2614

Katz, J.D., B. Wang, K. Haskins, C. Benoist, and D. Mathis. 1993. Following a diabetogenic T cell from genesis through pathogenesis. *Cell.* 74:1089–1100. https://doi.org/10.1016/0092-8674(93)90730-E

Katzman, S.D., W.E. O'Gorman, A.V. Villarino, E. Gallo, R.S. Friedman, M.F. Krummel, G.P. Nolan, and A.K. Abbas. 2010. Duration of antigen receptor signaling determines T-cell tolerance or activation. *Proc. Natl. Acad. Sci. USA.* 107:18085–18090. https://doi.org/10.1073/pnas.1010560107

Keir, M.E., S.C. Liang, I. Guleria, Y.E. Latchman, A. Qipo, L.A. Albacker, M. Koulmanda, G.J. Freeman, M.H. Sayegh, and A.H. Sharpe. 2006. Tissue expression of PD-L1 mediates peripheral T cell tolerance. *J. Exp. Med.* 203:883–895. https://doi.org/10.1084/jem.20051776

Klementowicz, J.E., A.E. Mahne, A. Spence, V. Nguyen, A.T. Satpathy, K.M. Murphy, and Q. Tang. 2017. Cutting Edge: Origins, Recruitment, and Regulation of CD11c$^+$ Cells in Inflamed Islets of Autoimmune Diabetes Mice. *J. Immunol.* 199:27–32. https://doi.org/10.4049/jimmunol.1601062

Krummel, M.F., F. Bartumeus, and A. Gérard. 2016. T cell migration, search strategies and mechanisms. *Nat. Rev. Immunol.* 16:193–201. https://doi.org/10.1038/nri.2015.16

Kurts, C., F.R. Carbone, M. Barnden, E. Blanas, J. Allison, W.R. Heath, and J.F. Miller. 1997. CD4$^+$ T cell help impairs CD8$^+$ T cell deletion induced by cross-presentation of self-antigens and favors autoimmunity. *J. Exp. Med.* 186:2057–2062. https://doi.org/10.1084/jem.186.12.2057

Larkin, J., V. Chiarion-Sileni, R. González, J.J. Grob, C.L. Cowey, C.D. Lao, D. Schadendorf, R. Dummer, M. Smylie, P. Rutkowski, et al. 2015. Combined Nivolumab and Ipilimumab or Monotherapy in Untreated Melanoma. *N. Engl. J. Med.* 373:23–34. https://doi.org/10.1056/NEJMoa1504030

Lindsay, R.S., K. Corbin, A. Mahne, B.E. Levitt, M.J. Gebert, E.J. Wigton, B.J. Bradley, K. Haskins, J. Jacobelli, Q. Tang, et al. 2015. Antigen recognition in the islets changes with progression of autoimmune islet infiltration. *J. Immunol.* 194:522–530. https://doi.org/10.4049/jimmunol.1400626

Liu, T., L. Zhang, D. Joo, and S.C. Sun. 2017. NF-κB signaling in inflammation. *Signal Transduct. Target. Ther.* 2:17023. https://doi.org/10.1038/sigtrans.2017.23

Lu, Q., and G. Lemke. 2001. Homeostatic regulation of the immune system by receptor tyrosine kinases of the Tyro 3 family. *Science.* 293:306–311. https://doi.org/10.1126/science.1061663

Lühder, F., P. Höglund, J.P. Allison, C. Benoist, and D. Mathis. 1998. Cytotoxic T lymphocyte-associated antigen 4 (CTLA-4) regulates the unfolding of autoimmune diabetes. *J. Exp. Med.* 187:427–432. https://doi.org/10.1084/jem.187.3.427

Luhder, F., C. Chambers, J.P. Allison, C. Benoist, and D. Mathis. 2000. Pinpointing when T cell costimulatory receptor CTLA-4 must be engaged to dampen diabetogenic T cells. *Proc. Natl. Acad. Sci. USA.* 97:12204–12209. https://doi.org/10.1073/pnas.200348397

Maimon, A., V. Levi-Yahid, K. Ben-Meir, A. Halpern, Z. Talmi, S. Priya, G. Mizraji, S. Mistriel-Zerbib, M. Berger, M. Baniyash, et al. 2021. Myeloid cell-derived PROS1 inhibits tumor metastasis by regulating inflammatory and immune responses via IL-10. *J. Clin. Invest.* 131:126089. https://doi.org/10.1172/JCI126089

McKee, A.S., M.A. Burchill, M.W. Munks, L. Jin, J.W. Kappler, R.S. Friedman, J. Jacobelli, and P. Marrack. 2013. Host DNA released in response to aluminum adjuvant enhances MHC class II-mediated antigen presentation and prolongs CD4 T-cell interactions with dendritic cells. *Proc. Natl. Acad. Sci. USA.* 110:E1122–E1131. https://doi.org/10.1073/pnas.1300392110

Melli, K., R.S. Friedman, A.E. Martin, E.B. Finger, G. Miao, G.L. Szot, M.F. Krummel, and Q. Tang. 2009. Amplification of autoimmune response through induction of dendritic cell maturation in inflamed tissues. *J. Immunol.* 182:2590–2600. https://doi.org/10.4049/jimmunol.0803543

Meredith, M.M., K. Liu, G. Darrasse-Jeze, A.O. Kamphorst, H.A. Schreiber, P. Guermonprez, J. Idoyaga, C. Cheong, K.-H. Yao, R.E. Niec, and M.C. Nussenzweig. 2012. Expression of the zinc finger transcription factor zDC (Zbtb46, Btbd4) defines the classical dendritic cell lineage. *J. Exp. Med.* 209:1153–1165. https://doi.org/10.1084/jem.20112675

Mohan, J.F., R.H. Kohler, J.A. Hill, R. Weissleder, D. Mathis, and C. Benoist. 2017. Imaging the emergence and natural progression of spontaneous autoimmune diabetes. *Proc. Natl. Acad. Sci. USA.* 114:E7776–E7785. https://doi.org/10.1073/pnas.1707381114

Myers, K.V., S.R. Amend, and K.J. Pienta. 2019. Targeting Tyro3, Axl and MerTK (TAM receptors): implications for macrophages in the tumor microenvironment. *Mol. Cancer.* 18:94. https://doi.org/10.1186/s12943-019-1022-2

Nagata, K., K. Ohashi, T. Nakano, H. Arita, C. Zong, H. Hanafusa, and K. Mizuno. 1996. Identification of the product of growth arrest-specific gene 6 as a common ligand for Axl, Sky, and Mer receptor tyrosine kinases. *J. Biol. Chem.* 271:30022–30027. https://doi.org/10.1074/jbc.271.47.30022

Nakano, T., Y. Ishimoto, J. Kishino, M. Umeda, K. Inoue, K. Nagata, K. Ohashi, K. Mizuno, and H. Arita. 1997. Cell adhesion to phosphatidylserine mediated by a product of growth arrest-specific gene 6. *J. Biol. Chem.* 272:29411–29414. https://doi.org/10.1074/jbc.272.47.29411

Peeters, M.J.W., D. Dulkeviciute, A. Draghi, C. Ritter, A. Rahbech, S.K. Skadborg, T. Seremet, A.M. Carnaz Simões, E. Martinenaite, H.R. Halldórsdóttir, et al. 2019. MERTK Acts as a costimulatory receptor on human cd8 t cells. *Cancer Immunol. Res.* 7:1472–1484. https://doi.org/10.1158/2326-6066.CIR-18-0841

Rothlin, C.V., E.A. Carrera-Silva, L. Bosurgi, and S. Ghosh. 2015. TAM receptor signaling in immune homeostasis. *Annu. Rev. Immunol.* 33:355–391. https://doi.org/10.1146/annurev-immunol-032414-112103

Sandor, A.M., R.S. Lindsay, N. Dyjack, J.C. Whitesell, C. Rios, B.J. Bradley, K. Haskins, D.V. Serreze, A.M. Geurts, Y.G. Chen, et al. 2019. CD11c^{+} cells are gatekeepers for lymphocyte trafficking to infiltrated islets during type 1 diabetes. *Front. Immunol.* 10:99. https://doi.org/10.3389/fimmu.2019.00099

Saxena, V., J.K. Ondr, A.F. Magnusen, D.H. Munn, and J.D. Katz. 2007. The countervailing actions of myeloid and plasmacytoid dendritic cells control autoimmune diabetes in the nonobese diabetic mouse. *J. Immunol.* 179:5041–5053. https://doi.org/10.4049/jimmunol.179.8.5041

Scott, R.S., E.J. McMahon, S.M. Pop, E.A. Reap, R. Caricchio, P.L. Cohen, H.S. Earp, and G.K. Matsushima. 2001. Phagocytosis and clearance of apoptotic cells is mediated by MER. *Nature.* 411:207–211. https://doi.org/10.1038/35075603

Sen, P., M.A. Wallet, Z. Yi, Y. Huang, M. Henderson, C.E. Mathews, H.S. Earp, G. Matsushima, A.S. Baldwin Jr., and R.M. Tisch. 2007. Apoptotic cells induce Mer tyrosine kinase-dependent blockade of NF-kappaB activation in dendritic cells. *Blood.* 109:653–660. https://doi.org/10.1182/blood-2006-04-017368

Shakhar, G., R.L. Lindquist, D. Skokos, D. Dudziak, J.H. Huang, M.C. Nussenzweig, and M.L. Dustin. 2005. Stable T cell-dendritic cell interactions precede the development of both tolerance and immunity in vivo. *Nat. Immunol.* 6:707–714. https://doi.org/10.1038/ni1210

Sinik, L., K.A. Minson, J.J. Tentler, J. Carrico, S.M. Bagby, W.A. Robinson, R. Kami, T. Burstyn-Cohen, S.G. Eckhardt, X. Wang, et al. 2019. Inhibition of MERTK Promotes Suppression of Tumor Growth in BRAF Mutant and BRAF Wild-Type Melanoma. *Mol. Cancer Ther.* 18:278–288. https://doi.org/10.1158/1535-7163.MCT-18-0456

Tadokoro, C.E., G. Shakhar, S. Shen, Y. Ding, A.C. Lino, A. Maraver, J.J. Lafaille, and M.L. Dustin. 2006. Regulatory T cells inhibit stable contacts between CD4^{+} T cells and dendritic cells in vivo. *J. Exp. Med.* 203:505–511. https://doi.org/10.1084/jem.20050783

Tamoutounour, S., M. Guilliams, F. Montanana Sanchis, H. Liu, D. Terhorst, C. Malosse, E. Pollet, L. Ardouin, H. Luche, C. Sanchez, et al. 2013. Origins and functional specialization of macrophages and of conventional and monocyte-derived dendritic cells in mouse skin. *Immunity.* 39:925–938. https://doi.org/10.1016/j.immuni.2013.10.004

Tang, Q., E.K. Boden, K.J. Henriksen, H. Bour-Jordan, M. Bi, and J.A. Bluestone. 2004a. Distinct roles of CTLA-4 and TGF-beta in CD4^{+}CD25^{+} regulatory T cell function. *Eur. J. Immunol.* 34:2996–3005. https://doi.org/10.1002/eji.200425143

Tang, Q., K.J. Henriksen, M. Bi, E.B. Finger, G. Szot, J. Ye, E.L. Masteller, H. McDevitt, M. Bonyhadi, and J.A. Bluestone. 2004b. In vitro-expanded antigen-specific regulatory T cells suppress autoimmune diabetes. *J. Exp. Med.* 199:1455–1465. https://doi.org/10.1084/jem.20040139

Tang, Q., J.Y. Adams, A.J. Tooley, M. Bi, B.T. Fife, P. Serra, P. Santamaria, R.M. Locksley, M.F. Krummel, and J.A. Bluestone. 2006. Visualizing regulatory T cell control of autoimmune responses in nonobese diabetic mice. *Nat. Immunol.* 7:83–92. https://doi.org/10.1038/ni1289

Tarbell, K.V., L. Petit, X. Zuo, P. Toy, X. Luo, A. Mqadmi, H. Yang, M. Suthanthiran, S. Mojsov, and R.M. Steinman. 2007. Dendritic cell-expanded, islet-specific CD4^{+} CD25^{+} CD62L^{+} regulatory T cells restore normoglycemia in diabetic NOD mice. *J. Exp. Med.* 204:191–201. https://doi.org/10.1084/jem.20061631

Tonkin, D.R., and K. Haskins. 2009. Regulatory T cells enter the pancreas during suppression of type 1 diabetes and inhibit effector T cells and macrophages in a TGF-beta-dependent manner. *Eur. J. Immunol.* 39:1313–1322. https://doi.org/10.1002/eji.200838916

Topalian, S.L., F.S. Hodi, J.R. Brahmer, S.N. Gettinger, D.C. Smith, D.F. McDermott, J.D. Powderly, R.D. Carvajal, J.A. Sosman, M.B. Atkins, et al. 2012. Safety, activity, and immune correlates of anti-PD-1 antibody in cancer. *N. Engl. J. Med.* 366:2443–2454. https://doi.org/10.1056/NEJMoa1200690

Turley, S., L. Poirot, M. Hattori, C. Benoist, and D. Mathis. 2003. Physiological beta cell death triggers priming of self-reactive T cells by dendritic cells in a type-1 diabetes model. *J. Exp. Med.* 198:1527–1537. https://doi.org/10.1084/jem.20030966

van der Meer, J.H.M., T. van der Poll, and C. van 't Veer. 2014. TAM receptors, Gas6, and protein S: roles in inflammation and hemostasis. *Blood.* 123:2460–2469. https://doi.org/10.1182/blood-2013-09-528752

van Megen, K.M., M.P. Spindler, F.M. Keij, I. Bosch, F. Sprangers, A. van Royen-Kerkhof, T. Nikolic, and B.O. Roep. 2017. Relapsing/remitting type 1 diabetes. *Diabetologia.* 60:2252–2255. https://doi.org/10.1007/s00125-017-4403-3

von Herrath, M., S. Sanda, and K. Herold. 2007. Type 1 diabetes as a relapsing-remitting disease? *Nat. Rev. Immunol.* 7:988–994. https://doi.org/10.1038/nri2192

Wallet, M.A., P. Sen, R.R. Flores, Y. Wang, Z. Yi, Y. Huang, C.E. Mathews, H.S. Earp, G. Matsushima, B. Wang, and R. Tisch. 2008. MerTK is required for apoptotic cell-induced T cell tolerance. *J. Exp. Med.* 205:219–232. https://doi.org/10.1084/jem.20062293

Wallet, M.A., R.R. Flores, Y. Wang, Z. Yi, C.J. Kroger, C.E. Mathews, H.S. Earp, G. Matsushima, B. Wang, and R. Tisch. 2009. MerTK regulates thymic selection of autoreactive T cells. *Proc. Natl. Acad. Sci. USA.* 106:4810–4815. https://doi.org/10.1073/pnas.0900683106

Wu, G., Z. Ma, Y. Cheng, W. Hu, C. Deng, S. Jiang, T. Li, F. Chen, and Y. Yang. 2018a. Targeting Gas6/TAM in cancer cells and tumor microenvironment. *Mol. Cancer.* 17:20. https://doi.org/10.1186/s12943-018-0769-1

Wu, J., L.N. Frady, R.E. Bash, S.M. Cohen, A.N. Schorzman, Y.T. Su, D.M. Irvin, W.C. Zamboni, X. Wang, S.V. Frye, et al. 2018b. MerTK as a therapeutic target in glioblastoma. *Neuro-oncol.* 20:92–102. https://doi.org/10.1093/neuonc/nox111

Yin, N., J. Xu, F. Ginhoux, G.J. Randolph, M. Merad, Y. Ding, and J.S. Bromberg. 2012. Functional specialization of islet dendritic cell subsets. *J. Immunol.* 188:4921–4930. https://doi.org/10.4049/jimmunol.1103725

Zakharov, P.N., H. Hu, X. Wan, and E.R. Unanue. 2020. Single-cell RNA sequencing of murine islets shows high cellular complexity at all stages of autoimmune diabetes. *J. Exp. Med.* 217:e20192362. https://doi.org/10.1084/jem.20192362

Zhang, W., D. DeRyckere, D. Hunter, J. Liu, M.A. Stashko, K.A. Minson, C.T. Cummings, M. Lee, T.G. Glaros, D.L. Newton, et al. 2014. UNC2025, a potent and orally bioavailable MER/FLT3 dual inhibitor. *J. Med. Chem.* 57:7031–7041. https://doi.org/10.1021/jm500749d

Zhang, B., H. Wu, L. Fang, P. Ding, K. Xu, Q. Yang, and R. Liu. 2017. MerTK Does Not Mediate Phagocytosis of Staphylococcus aureus but Attenuates Inflammation Induced by Staphylococcal Lipoteichoic Acid Through Blocking NF-κB Activation. *Inflammation.* 40:1543–1552. https://doi.org/10.1007/s10753-017-0595-4

Zhou, Y., M. Fei, G. Zhang, W.C. Liang, W. Lin, Y. Wu, R. Piskol, J. Ridgway, E. McNamara, H. Huang, et al. 2020. Blockade of the Phagocytic Receptor MerTK on Tumor-Associated Macrophages Enhances P2X7R-Dependent STING Activation by Tumor-Derived cGAMP. *Immunity.* 52:357–373.e9. https://doi.org/10.1016/j.immuni.2020.01.014

Supplemental material

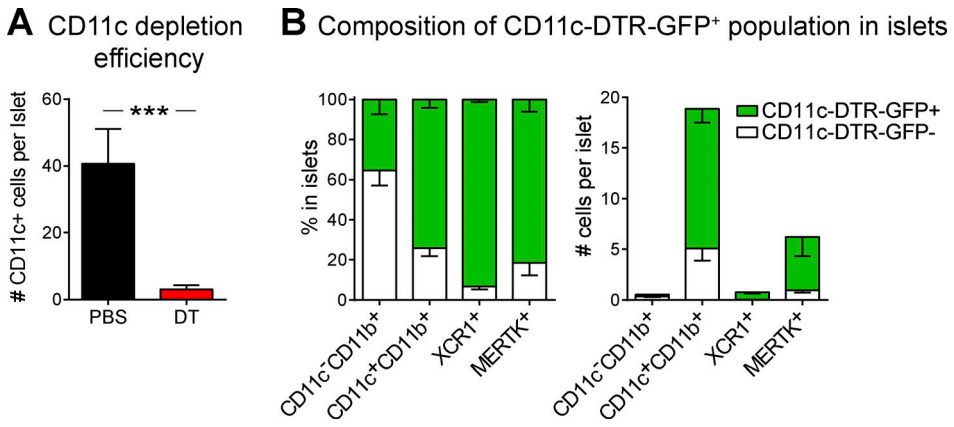

Figure S1. **CD11c-DTR-GFP cells are effectively depleted in the islets and include CD11b$^+$, XCR1$^+$, and MERTK$^+$ populations.** NOD.CD11c-DTR-GFP BM chimeras containing NOD.CD11c-DTR-GFP BM were treated twice with PBS or DT. **(A and B)** Islets from treated NOD.CD11c-DTR BM chimeras (A) or NOD.CD11c-DTR-GFP$^+$CD2.dsRed$^+$ female mice (B) were isolated, digested and dissociated, stained, and analyzed by flow cytometry. **(A)** Quantification of CD11c$^+$ cells in islets following PBS or DT treatment. **(B)** Quantification of the composition of the CD11c-DTR-GFP$^+$ versus GFP$^-$ mononuclear phagocytes in the islets. **(A)** n = 12 mice (PBS), n = 16 mice (DT) from seven independent experiments. Error bars represent SEM. Statistics: Student's t test; ***, P < 0.001. **(B)** n = 4 mice from three independent experiments.

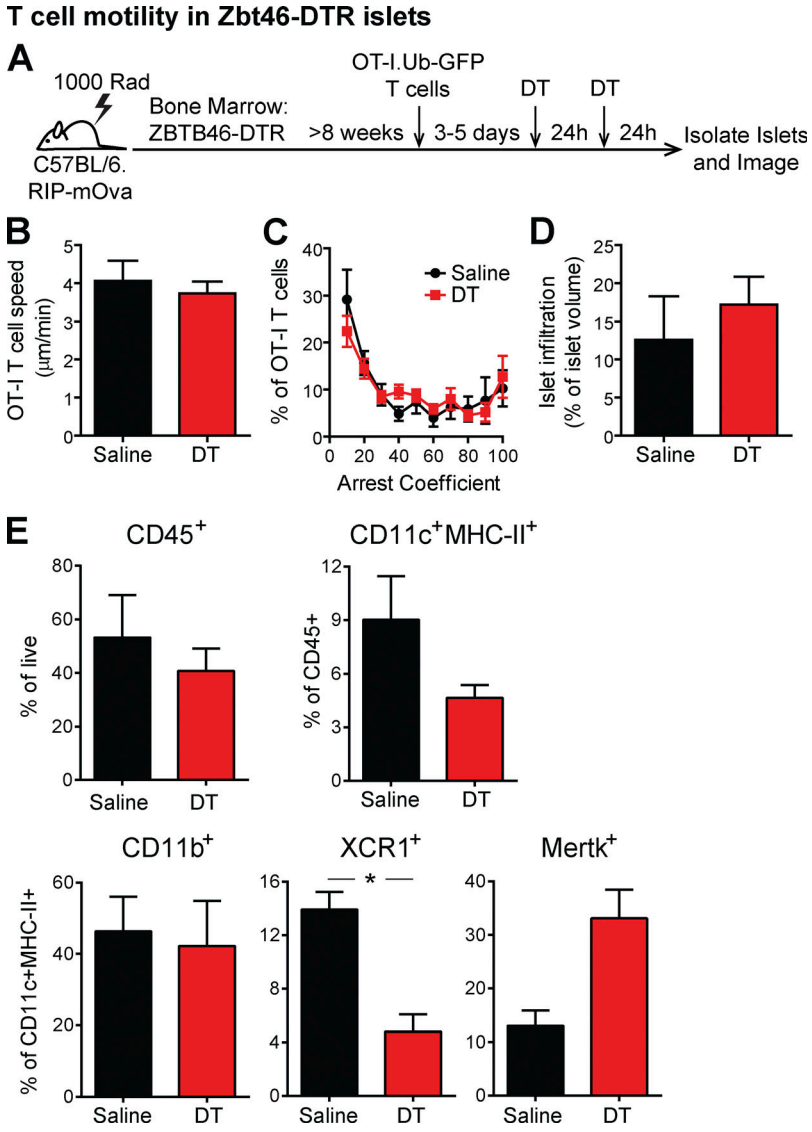

Figure S2. **Zbtb46-expressing DCs are not the subset of CD11c⁺ cells in islets that prevent T cell arrest. (A–D)** Islet infiltration was induced in B6.Zbtb46-DTR.RIP-mOva BM chimeras by the transfer of naive OT-I.GFP T cells. **(A)** 3–5 d after T cell transfer, the chimeras were treated twice with PBS (control) or DT (Zbtb46 depleted). 48 h after treatment initiation, T cell motility was analyzed in explanted islets by two-photon microscopy. **(B)** Average T cell crawling speed per islet. **(C)** Arrest coefficient: percentage of time a T cell is moving <1.5 µm/min. **(D)** Average islet infiltration levels. **(E)** Flow cytometric analysis of mononuclear phagocytes in the islets of PBS (control)– or DT (Zbtb46-depleted)–treated NOD.Zbtb46-DTR BM chimeras, 48 h after treatment initiation. **(A–D)** Data were pooled from three independent experiments. *n* = 10 islets from PBS-treated mice and 26 islets from DT-treated mice. **(E)** Data were pooled from four or five mice per condition in two independent experiments. **(B, D, and E)** Statistics: Student's t test. **(C)** Statistics: two-way ANOVA. Error bars represent SEM. **(B–E)** Error bars represent SEM. *, P < 0.05.

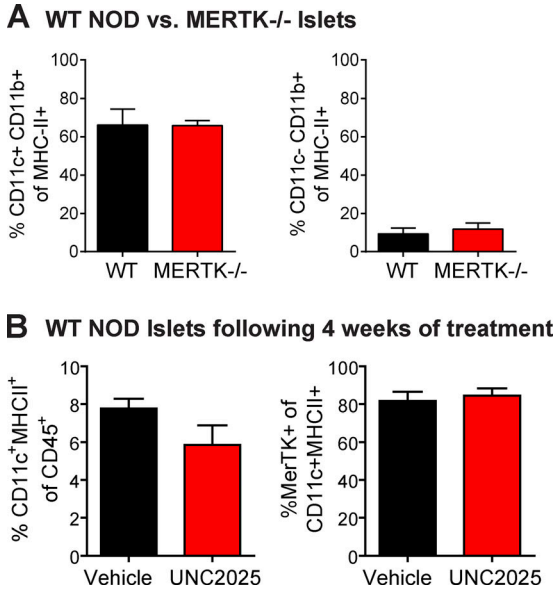

Figure S3. **Mononuclear phagocyte frequency in islets is not altered by MERTK deficiency or MERTK inhibition. (A)** Cell frequency of WT and MERTK$^{-/-}$ NOD mice was quantified in the islets by flow cytometry. Statistics: two-tailed Student's t test. *n* = 3 experiments. Error bars represent SEM. **(B)** WT NOD female mice were treated with 30 mg/kg UNC2025 or saline vehicle twice daily by oral gavage for 4 wk. Cell frequency was quantified in the islets by flow cytometry. Statistics: two-tailed Student's t test. *n* = 6–8 mice per group from two experiments. Error bars represent SEM.

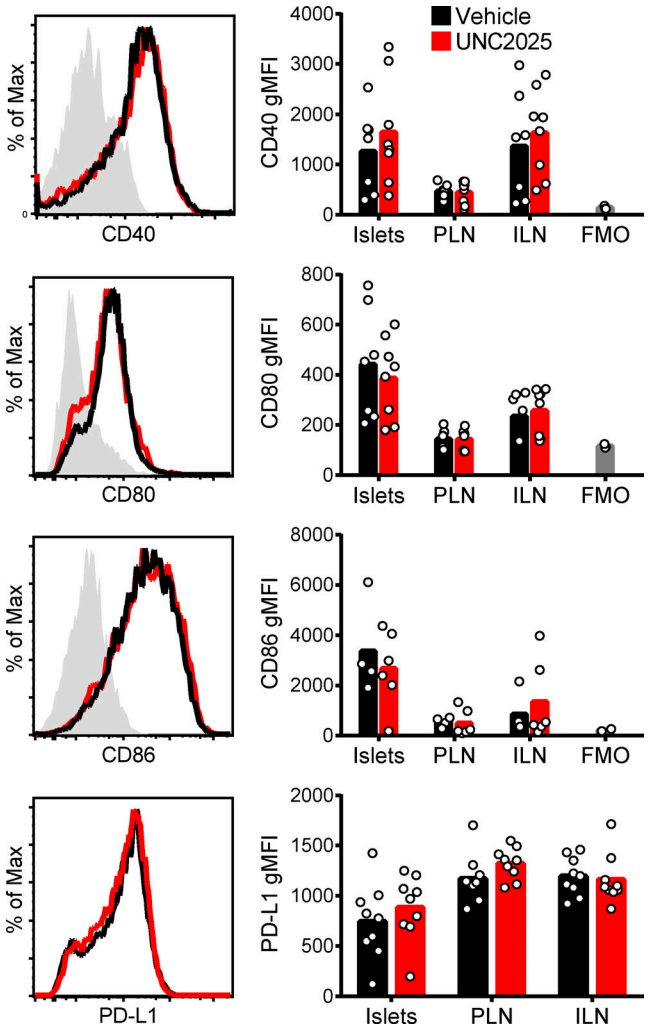

Figure S4. **MERTK inhibition does not alter the expression of islet costimulatory or coinhibitory ligands.** WT NOD female mice were treated with 30 mg/kg UNC2025 or saline vehicle for 18 h. Islets, PLNs, and ILNs were then harvested, dissociated, antibody stained, and analyzed by flow cytometry. Data show expression on $CD45^+CD11c^+$ cells. *n* = 3–8 mice from two to four experiments. FMO, fluorescence minus one, unstained geometric MFI (gMFI) of gated population.

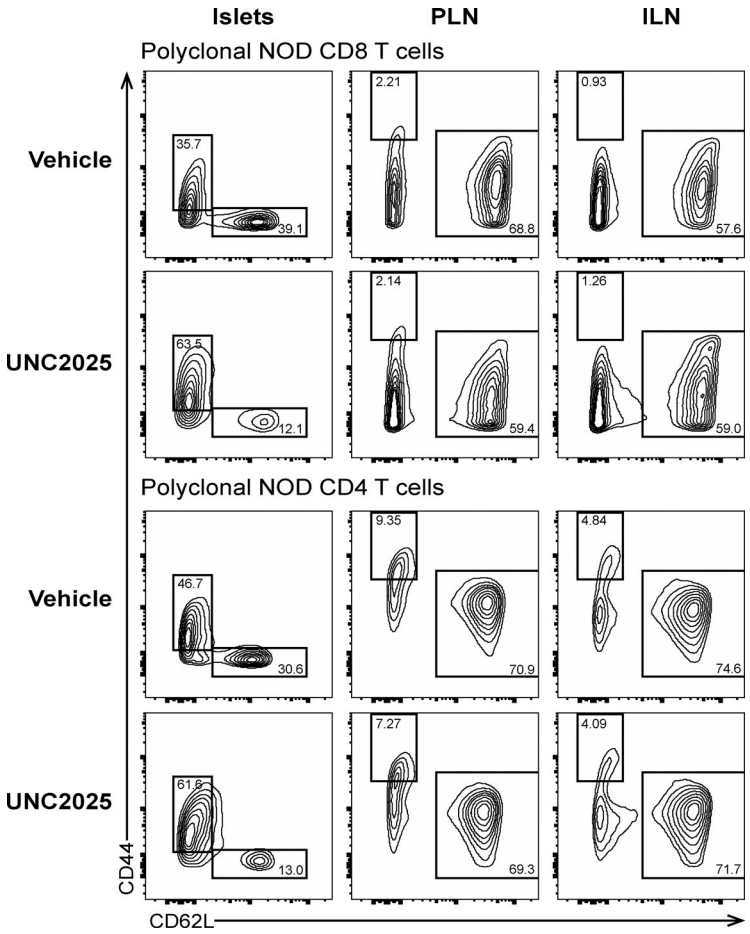

Figure S5. **Examples of CD44/CD62L flow cytometry plots after vehicle or UNC2025 treatment.** Data quantified in Fig. 7 A. WT NOD female mice were treated with 30 mg/kg UNC2025 or vehicle twice by oral gavage. Islets and LNs were isolated 17h after treatment initiation, digested, stained and analyzed by flow cytometry. Gating of islet samples was done independently from gating of LN samples due to partial cleavage of CD44 by Collagenase P, which was used for the islet isolation. Previous tests treating split samples of splenocytes with Collagenase P under the conditions used for islet isolation compared with no Collagenase P showed diminished florescence intensity of CD44 but equal frequencies when gating was adjusted. CD44 gates were set for islet samples and LN samples using $CD62L^+$ cells as a $CD44^-$ population.

Video 1. **$CD11c^+$ cells in islets prevent T cell arrest.** NOD.CD11c-DTR BM chimeras containing 90% NOD.CD11c-DTR BM + 10% NOD.CD11c-DTR.8.3.CD2-dsRed BM were treated twice with PBS (intact) or DT (CD11c depleted). 48 h after treatment initiation, T cell motility was analyzed in explanted islets by two-photon microscopy. Representative islet movies from PBS control– or DT-treated mice with 10-min tracks of motion. 8.3 T cells are shown in white, and CD11c-DTR-GFP is shown in green. Dashed line depicts islet border. Time, minutes:seconds; scale bar, 50 µm. 5 frames/sec. Representative of data quantified in Fig. 1, A–G.

Video 2. **Islet-antigen–specific T cells in $MERTK^{-/-}$ islets show decreased motility and increased T cell arrest.** Activated BDC-2.5 CD4 T cells were transferred into NOD or NOD.$MERTK^{-/-}$ female mice to initiate islet infiltration. Fluorescently labeled activated 8.3 CD8 T cells (white) and BDC-2.5 CD4 T cells (red) were then transferred into the same mice 3–6 d later. 24 h after fluorescent T cell transfer, islets were isolated and analyzed by two-photon microscopy. Representative islet movies from WT NOD or NOD.$MERTK^{-/-}$ mice with 10-min tracks of motion. Dashed line depicts islet border. Time, minutes:seconds; scale bar, 50 µm. 5 frames/sec. Representative of data quantified in Fig. 3.

Video 3. **MERTK signaling prevents T cell arrest in a solid tumor model.** B78ChOva tumor cells were implanted in C57BL/6 or C57BL/6.MERTK$^{-/-}$ mice. Activated OT-I.Ubiquitin-GFP CD8 T cells (green) were then transferred into tumor bearing mice 4–6 d later. 5–7 d after fluorescent T cell transfer, mice were treated with UNC2025 or vehicle. 18 h after treatment, tumors were excised and analyzed by two-photon microscopy. Representative movies of OT-I T cell (green) motility on the tumor surface with 10-min tracks of motion. Collagen (blue) delineates the tumor surface. Time, minutes:seconds; scale bar, 50 µm. 6 frames/sec. Representative of data quantified in Fig. 5.

Video 4. **MERTK signaling prevents islet T cell–APC interactions in an antigen-dependent manner.** Fluorescently labeled, activated 8.3 CD8 T cells (white), BDC-2.5 CD4 T cells (red), and polyclonal T cells (blue) were cotransferred into female NOD.CD11c-YFP (green) mice. Mice were treated twice daily with saline vehicle or 30 mg/kg UNC2025, a small-molecule inhibitor of MERTK and Flt3. 16 h following the initial treatment, islets were isolated and analyzed by two-photon microscopy. Representative islet movies from vehicle- or UNC2025-treated mice with 5-min tracks of motion and circles highlighting sustained interactions between T cells and APCs. Time, minutes:seconds; scale bar, 30 µm. 6 frames/sec. Representative of data quantified in Figs. 4 and 6.

Table S1 is provided online and summarizes nPOD donor information.